European Journal of Mechanics B/Fluids 29 (2010) 61–83

Contents lists available at ScienceDirect

European Journal of Mechanics B/Fluids

journal homepage: www.elsevier.com/locate/ejmflu

Steady and unsteady Görtler boundary-layer instability on concave wall

A.V. Boiko, A.V. Ivanov, Y.S. Kachanov*, D.A. Mischenko

Khristianovich Institute of Theoretical and Applied Mechanics, Institutskaya str. 4/1, 630090 Novosibirsk, Russian Federation

ARTICLE INFO

Article history:
Received 1 November 2008
Received in revised form
20 July 2009
Accepted 2 November 2009
Available online 11 November 2009

ABSTRACT

The subject of the present combined experimental and theoretical investigation is the steady and unsteady linear Görtler instability. The majority of previous experiments were devoted to the steady Görtler vortices, despite the unsteady ones are also observed in real transitional flows. Moreover, even for the steady Görtler vortices no quantitative agreement between the experimental and theoretical linear-stability characteristics was obtained, especially for disturbance amplification rates. The experimental difficulties were connected, in particular, with a rather poor accuracy of measurements at zero disturbance frequency, a possible influence of nonlinearity, and an admixture of non-modal (transient) growth mechanism. All these difficulties have been overcome in the experimental part of the present study by means of: (*i*) tuning-out of the exact zero frequency of Görtler vortices and working, instead, with quasi-steady perturbations of very low frequencies, (*ii*) performing measurements at low disturbance amplitudes, and (*iii*) minimization and careful estimation of the disturbance-source near-field by means of utilizing a special controlled disturbance source and performing special numerical computations for exact experimental conditions. A detailed study of all linear-stability characteristics for *essentially unsteady* Görtler vortices was performed in this paper as well. The results are obtained in a range of Görtler numbers $13 \lesssim G\ddot{o} \lesssim 17.3$, frequency parameters $F = 0.56$–22.70, and spanwise wavelength parameters $\Lambda = 149$–775 (close to the most amplified Görtler modes).

Appropriate calculations based on locally-parallel and non-local non-parallel linear-stability theories were performed and compared quantitatively with experimentally obtained linear-stability characteristics. For the first time all stability characteristics measured for steady Görtler vortices (in quasi-steady regimes) are found to agree very well with those calculated for the most amplified first discrete-spectrum mode of the linear Görtler-instability problem. Similar good agreement is obtained for essentially unsteady Görtler vortices. The roles of effects of the base-flow non-parallelism and the disturbance-source near-field are examined.

1. Introduction

Görtler instability (or Taylor–Görtler one in closed rotating streams) is widely spread in various shear-flows. In particular, it is often observed in boundary layers developing over concave walls in a wide range of free-stream speeds and Mach numbers [1]. This instability leads to amplification of streamwise elongated vortices (steady or/and unsteady). Due to its great importance the problem of Görtler instability is being investigated for a long time experimentally, theoretically, and numerically (see, e.g., reviews in Ref. [2–4]). Great majority of these studies are devoted to *steady* Görtler vortices.

For the first time the streamwise vortices, associated with an instability of a shear-flow between two rotating cylinders, were found and studied both theoretically and experimentally by Taylor [5]. Experiments [6] showed that the laminar boundary layers over concave walls become turbulent at lower Reynolds numbers than those over flat or convex surfaces. Later Görtler [7] adopted the approach of local parallelism of boundary layer streamlines and used normal-mode analysis to show that the instability can occur in boundary layers over concave surfaces when a certain parameter (the Görtler number)

$$G\ddot{o} = \mathrm{Re}\sqrt{\frac{\delta}{R}}, \tag{1}$$

exceeds a critical value. Here Reynolds number is defined as $Re = U_e\delta/\nu$, the length δ characterizes the boundary-layer thickness, U_e is the free-stream velocity at the boundary-layer edge, ν denotes the kinematic viscosity of the fluid, and R is the radius of wall curvature. The critical Görtler number changes with the disturbance spanwise wavenumber β (normalized usually by the length

* Corresponding author. Tel.: +7 383 3304278; fax: +7 383 3307268.
E-mail address: kachanov@itam.nsc.ru (Y.S. Kachanov).

0997-7546/$ – see front matter © 2009 Elsevier Masson SAS. All rights reserved.
doi:10.1016/j.euromechflu.2009.11.001

scale δ). The dependence Gö(β) forms a neutral stability curve defined in the ($G\ddot{o}$,β) -plane. Throughout this paper, if other is not specified, we assume that the length scale is equivalent to the boundary-layer displacement thickness.

A relation of the early flow turbulization found in Ref. [6] to the Görtler instability was demonstrated by Liepmann [8]. First direct experimental evidence of existence of steady Görtler vortices was obtained by china-clay surface visualization in Ref. [9] and by hot-wire measurements in the flow in Ref. [10]. The experiments and subsequent analysis showed that the instability develops in space and has the convective character. Later numerous flow visualizations and hot-wire measurements (see, e.g., Ref. [11]) helped to improve significantly the understanding of this phenomenon and to evaluate its influence on the laminar–turbulent transition in boundary layers.

A series of studies was performed with excitation of controlled perturbations. In such experiments [12] performed in water some spanwise periodic steady disturbances were introduced into a boundary layer by means of an array of heated streamwise-oriented wires. The instability was detected via an observation of deformation of spanwise time-lines formed by hydrogen bubbles. Some points belonging to a short-wave part of the neutral stability curve were obtained. However, the amplitudes of the excited disturbances were quite large because it would be otherwise difficult to detect them by means of the used visualization method. In experiments of Ref. [13,14] a set of thin plates located in free stream was used to generate steady Görtler vortices; some of the results obtained in Ref. [12] were reproduced and also additional points of the neutral stability curve were documented.

However, the disturbance growth rates obtained experimentally did not agree with those calculated by the linear-stability theory in the whole range of spanwise wavenumbers and Görtler numbers studied [3,15]. One of the causers of the discrepancy was associated with nonlinear effects because the amplitudes of the streamwise velocity variations caused by the investigated vortices were quite large (often about 10% of free-stream speed, as in Ref. [12]). Another cause is related to the so-called transient growth of perturbations occurred in the disturbance-source near-field (see below).

In the long-wave region some serious difficulties exist in the linear-stability theory as well. For instance, in Ref. [7,16] the Görtler number of the neutral point increases as the spanwise-wavenumber decreases below 0.1 (when it is normalized by δ^*) and approaches 10 at wavenumber about 0.01. Meanwhile, in calculations of Ref. [17,18] the same Görtler number remains small and nearly constant (about 0.7–0.8), while in Ref. [19] it continues to decrease at least down to 0.1.

A great number of subsequent attempts to improve the theory by means of accounting for the boundary layer growth did not lead to an adequate solution of the problem. The disturbance growth rates predicted by various theories still differ significantly from each other and, what is of the most importance, disagree with the experimental data. Although according to the linear-stability theory [19] the flow becomes unstable when Görtler number exceeds value of about unity, the experimentalists were not able to observe Görtler vortices until $G\ddot{o}^* \approx 10$ (here and below we denote Görtler number $G\ddot{o}^*$ when displacement thickness δ^* is used as δ). The significant distinction of predicted and experimental growth rates is observed in the whole studied range of spanwise wavenumbers and Görtler numbers.

Hall [20,21] showed that the reduction of the problem under consideration to a set of homogeneous ordinary differential equations is not justified for values of Gö and $\beta \lesssim \mathcal{O}(1)$: the neglect of the downstream variation of the vortex shape (i.e. consideration of the wall-normal amplitude function as independent of x and prehistory of its development) is invalid in this case. To account for the prehistory, one has to formulate the problem as a set of partial differential equations and solve the corresponding parabolic initial-boundary-value problem. Corresponding numerical tests show that the behavior of stationary vortices at small Görtler numbers depends sufficiently on initial conditions and determination of a unique neutral stability curve loses practical significance [22–24]. In such a case most accurate approach, which allows one to trace the development of the vortices from very beginning, consists in formulating and solving the receptivity problem to provide proper initial conditions. However, this has been done only theoretically for Görtler vortices induced by a stationary roughness [25,26]. Experimentally receptivity of the Görtler vortices has not been considered up to now due to its complexity.

The situation in boundary layers (at least in the present experiment, where disturbance source is located at $G\ddot{o} = 0$) is aggravated also by the presence of a so-called 'near-field' region downstream of a disturbance source even at $\beta \gtrsim 1$ [27,28]. This phenomenon is related to the so-called *lift-up* effect [29], which allows for the streamwise disturbance velocity to experience a transient algebraic (rather than exponential) growth even in a linearly stable flow. This can be illustrated in terms of a large number of attenuating modes of linearized Navier–Stokes equations with the same value of the spanwise wavenumber and (possibly zero) frequency, but with different streamwise wavenumbers [30]. The superposition of the non-orthogonal modes produced by a disturbance source can lead to a complicated behavior (including a temporary growth) of the streamwise-velocity disturbance in an extended downstream area. The wall-normal profiles of the streamwise component of velocity disturbance resemble often for such perturbations the Görtler vortex profiles. This renders difficult to distinguish these two types of disturbances in experiment.

The majority of problems occurred in previous experimental investigations of *steady* Görtler vortices is associated with a poor measurement accuracy of small velocity perturbations on the background of large mean shear-flow velocity accompanied by large wall-normal gradients. Also, some of the previous experimental difficulties can be attributed, at least partly, to a possible influence of nonlinearity and to the discussed above mechanism of non-modal disturbance development or, in other words, to a large extent of disturbance-source near-fields. Due to these reasons, an accurate (and even approximate, mostly) agreement between the experimental growth rates of steady Görtler vortices and those predicted by the linear-stability theory has never been achieved until now.

Experimental investigations of the linear Görtler-instability problem in *non-stationary* formulation are absent at present. The number of available theoretical and numerical results on time-periodic vortices is also quite restricted, though the original Görtler equations [7] are time-dependent. The growth of Görtler-instability modes in a form of unsteady, oscillating vortices as a primary state was considered in Ref. [20,31] for subsonic and in Ref. [32] for supersonic boundary layers. It was shown that the unsteady modes (periodic in time) are less amplified compared to steady ones. In Ref. [20] this result was obtained with accounting for the effects of the base-flow non-parallelism but only in the limit of infinitely large spanwise wavenumbers. The case of wavenumbers of order of unity (being of the greatest practical importance) has not been studied.

The *initial-boundary-value* problem of the development of *unsteady* disturbances in boundary layer at a concave wall has been considered by Bertolotti [33]. The study was mainly devoted to the development of Tollmien–Schlichting (TS) waves, therefore the Navier–Stokes equations were reduced and normalized quite differently compared to the initial-boundary-value problem for Görtler vortices formulated in Ref. [22]. Nevertheless, it was

pointed out that the curvature promotes amplification of both the Görtler vortices and the oblique TS-waves. Their instability regions were found to merge as the surface curvature grows.

Based on flow visualizations and theoretical results, it is believed usually that steady vortices dominate in the flows in presence of Görtler instability. This is plausible quite often, but cannot be rigorously justified for all practical cases. The unsteady vortices can be initiated by low-frequency vortical perturbations of incoming flows and seem to appear frequently in many practical situations (see, e.g., Ref. [34]). Such perturbations are typical, for example, in boundary layers on curved blades of turbomachines. Consequently, the apparent predominance of steady Görtler vortices in numerous experiments might be explained, e.g., by a stronger boundary-layer receptivity to these disturbances, or by larger dimensionless amplitudes of surface roughness or free-stream non-uniformities in comparison with amplitudes of surface vibrations or free-stream velocity fluctuations, rather than by their largest amplification rates. Such situation might be similar to the swept-wing boundary-layer instability, where less amplified stationary disturbances dominate frequently in the flow [35].

The investigation of *unsteady* Görtler instability (including the quasi-steady case) described in the present paper is not only of great fundamental and practical importance, but also of large methodological significance. In particular the quasi-steady approach and new source of fully controlled unsteady Görtler vortices represent significant new steps in the field of the Görtler instability research.

The main ideas of the experimental approach used in the present investigation of *steady* Görtler vortices are the following:

1. To tune-out from the exact zero frequency and to perform, instead, measurements for quasi-steady, very low-frequency perturbations, which correspond physically to stationary disturbances (including the disturbance stability characteristics), as shown below. In this case the accuracy of measurements can be improved very much (by several orders of magnitude) with the help of utilizing Fourier analysis.
2. To perform measurements at extremely low disturbance amplitudes in order to provide a guaranteed linearity of the stability problem under investigation and to check experimentally the presence of linearity in the studied cases.
3. To minimize, identify, and take into account the effects of the disturbance-source near-field.
4. To excite quasi-steady Görtler vortices by means of a special disturbance source (which is able to provide the above mentioned prerequisites) and to carry out special numerical calculations in order to estimate the near-field length and properties.

The simultaneous theoretical investigation of the steady problem of the linear Görtler instability represents also an important peculiarity of the present work. The boundary-layer instability to *essentially unsteady* Görtler vortices is investigated here as well, both experimentally and theoretically. In addition, the applicability of locally-parallel and non-parallel stability theories is analyzed in detail.

2. Experimental setup

The experiments were carried out in the low-turbulence subsonic wind-tunnel T–324 of the Khristianovich Institute of Theoretical and Applied Mechanics of the Siberian Branch of the Russian Academy of Sciences. The wind-tunnel test section has length of 4 m and square test section 1 × 1 m. At the present experimental conditions the free-stream turbulence level did not exceed 0.02% in the frequency range above 1 Hz.

The sketch of the experimental model is presented in Fig. 1. The model consisted of a supporting flat plate (*2*), a concave-wall insert (*3*), and an outlet section (*7*) to provide smooth outcome of the flow from the insert to the flat part of the model without boundary-layer separation. The concave-wall insert was started at $x = 311$ mm ($G\ddot{o}^* = 9.0$) and ended at $x = 1111$ mm $G\ddot{o}^* \approx 20.1$. The plexiglas flat plate of 10 mm thickness with an elliptic nose part was installed horizontally in the wind-tunnel test section under zero angle of attack. In order to minimize the streamwise pressure gradient over the concave surface, an adjustable wall bump (*4*) was mounted on the test-section ceiling. The wall-bump surface was adjusted practically parallel to the model surface on its concave section.

Unsteady controlled Görtler vortices were excited in the boundary layer upstream the concave section by a disturbance source VS-II (*8*) [36]. This source was used previously for excitation of TS-waves [37–39] and cross-flow instability waves [40]. The excitation unit of the source mounted in the experimental model is sketched in Fig. 2a. It consists of an insert with a spanwise slot (*2*) oriented normal to the free-stream direction and an array of tubes distributed uniformly along the slot with outlets located immediately under it. The disturbances are produced by weak harmonic in time fluctuations of air inside the tubes representing, in fact, an array of point-like sources.

The excitation unit was flush mounted in the supporting flat plate (*1*) at a distance of 207 mm downstream from its leading edge ($Re^* = 645$, where Re^* is the Reynolds number based on the boundary-layer displacement thickness δ^*). The slot had length of 164 mm, width of 0.2 mm and depth of 1 mm. 82 tubes with step of 2 mm were used in the array. Each tube was connected by a 5 m long plastic pipe to one of eight identical loudspeakers positioned outside the wind-tunnel and closed with covers. Each cover was equipped with 12 fittings for connection with the pipes. The speakers operated at relatively low frequencies (between 0.5 and 20 Hz) and, therefore, produced inside every pipe (and, hence, inside the slot) some small-amplitude blowing/suction air fluctuations rather than acoustic waves.

The input harmonic signal (with definite frequency, amplitude, and phase) to each of the speakers was produced by one of eight channels of an electronic unit of the disturbance source VS-II consisted of a block of specialized digital-to-analog converters (DAC) combined with power amplifiers. Each channel was able to generate its own signal (stored in the DAC ROM and composed of 2048 points) of virtually any desired shape. The signals were produced by a special PC program (uploaded into the ROM prior to the experiment) and played back during the signal generation at

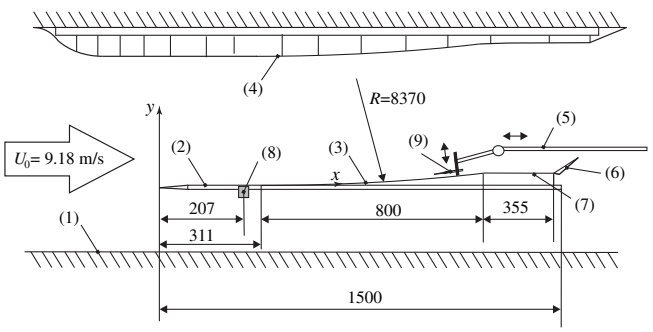

Fig. 1. Sketch of the experimental model: 1 — wall of wind-tunnel test section, 2 — supporting flat plate, 3 — concave insert with radius of curvature of 8.37 m, 4 — adjustable wall bump, 5 — traversing mechanism, 6 — flap, 7 — outlet section, 8 — disturbance source; 9 — hot-wire probe.

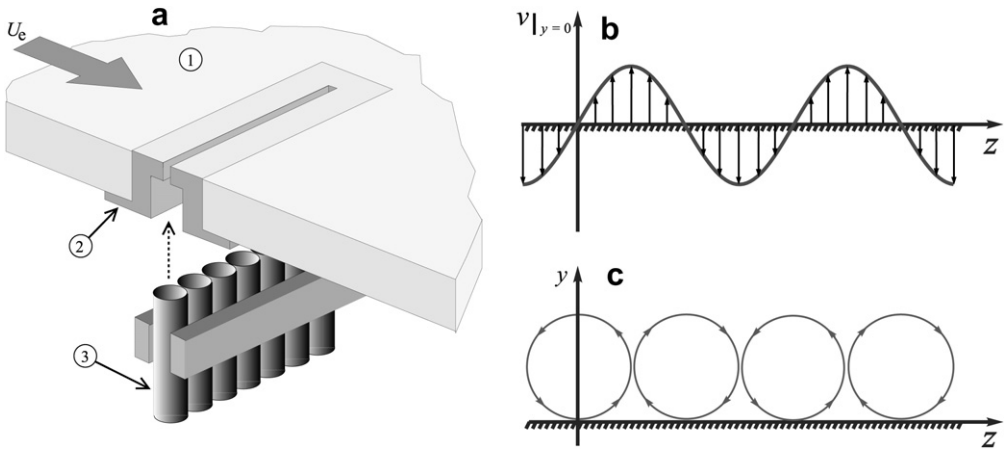

Fig. 2. Excitation unit of the disturbance source mounted in the experimental model (a); standing waves generated by the source (b) and a schematic plot of the Görtler vortices appearing downstream (c): 1 — surface of experimental model; 2 — slot insert; 3 — metal tubes.

a rate between 20 and 200 000 Hz controlled by an external clock generator.

A schematic diagram of the disturbance excitation is shown in the (y, z)-plane in Fig. 2b and c. The instantaneous spanwise distribution of the wall-normal velocity disturbance is presented in Fig. 2b, while the corresponding instantaneous sketch of the excited Görtler vortices is given in Fig. 2c.

Typical measured spanwise distributions of amplitude (A) and phase (φ) of boundary-layer perturbations excited by the source at 'initial' section $x = 397$ mm ($G^* = 10.3$) are illustrated in Fig. 3 for the spanwise wavelength $\lambda = 24$ mm ($\Lambda = 775$) at $f = 8$ Hz ($F = 9.08$). It is seen that the disturbances excited by the source correspond to a standing wave in the spanwise direction with the characteristic sine-type amplitude modulation and 180° phase jumps occurred at the amplitude minima. The distributions obtained in all other regimes under study looked similar. The results of their spatial Fourier transform give the spanwise-wavenumber spectrum consisted mainly of two modes with $\beta = \pm 2\pi/\lambda_z$. These quite pure standing waves turned out to be attributed to a system of unsteady counter-rotating Görtler vortices with one definite spanwise wavelength equal to λ_z (see below).

The intensity of the excitation was quite small in all studied regimes to provide generation of Görtler vortices with streamwise-velocity amplitudes less than 0.2–0.3% of the boundary-layer edge velocity (U_e) in the end of region of measurements (i.e. at $x = 892$ mm). So low disturbance amplitudes were used wittingly to provide a guaranteed linearity of the Görtler instability mechanism under study. It has become possible to study such low-amplitude perturbations due to a very good accuracy of their measurements, as far as the quasi-steady disturbances were utilized instead of the steady ones. Special measurements performed at varied initial amplitudes of the excited Görtler vortices have shown that their shapes (wall-normal profiles of phases and normalized amplitudes) and laws of downstream development are amplitude independent up to several percents of U_e. Thus, the experimentally measured Görtler vortex characteristics can be compared directly with those calculated based on *linear*-stability theories.

During main measurements the mean-flow velocity, total root-mean-square (rms) intensity of velocity fluctuations, and amplitudes and phases of frequency harmonics were obtained with the help of a constant temperature hot-wire anemometer AN–1003 produced by *AA Lab Systems*. The miniature single-wire probes used in the experiment were designed for boundary-layer measurements and made using technology by Kosorygin [41]. The probe consisted of a Wollaston-type wire (copper coated platinum) with a sensitive element of 0.3 mm length and 6 μm in diameter. The thirty-year experience of utilizing of such probes testifies that despite the rather low length-to-diameter aspect ratios they operate properly and measure accurately the streamwise-velocity component in boundary layers, providing in addition enhanced spatial resolution, which is very important for investigations of the spanwise-localized flow structures like the streamwise vortices under study.

In the used coordinate-system the x-axis is directed downstream and has its origin at the supporting plate leading edge; this coordinate is curvilinear and counted along the curved surface. The z-axis is oriented along the spanwise direction and y is wall-normal coordinate everywhere. All hot-wire signals corresponded to the streamwise (u –) component of the flow velocity. The hot-wire

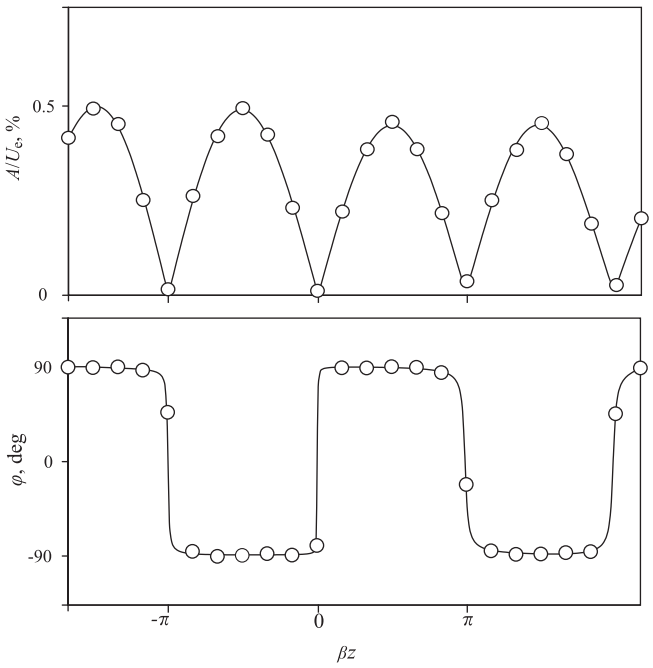

Fig. 3. Example of spanwise distributions of amplitudes and phases of boundary-layer disturbances excited by source VS-II at initial section $x = 397$ mm (○) approximated in plane of complex amplitudes by high-order polynomial (–). $\Lambda = 775$, $F = 9.08$, $G^* = 10.3$.

probe was mounted on a three-component traversing mechanism 5 (Fig. 1), which provided the spatial probe positioning with accuracy of ± 0.2 mm along z and x, and ±0.005 mm along y-coordinate.

Main boundary-layer measurements were carried out in a ranges of x between 300 and 900 mm and z between ±140 mm. During measurements of streamwise and spanwise distributions, the dimensionless wall-normal distance was fixed and equal to $y/\delta^* \approx 1.1$ (the corresponding dimensionless flow velocity was $U/U_e = 0.6$). This distance corresponds approximately to the wall-normal location of the amplitude maximum of the distance corresponded to the first Görtler-instability mode (see Sections. 5 and 6.1 below).

The hot-wire anemometer signal, as well as output signals of a resistive temperature detector and an electronic manometer measured the base-flow characteristics, were transferred into a PC synchronously with the reference signal produced by the disturbance source via an eight channel BNC–2120 connector and a 16-bit analog-to-digital convertor PCI–6035E by National Instruments. The data acquisition and linearization of the hot-wire signals were performed by a program implemented in MATLAB using King's law constants obtained during the probe calibration performed in the same wind-tunnel just prior to the measurements.

The linearized hot-wire signal was ensemble averaged synchronously with the disturbance source reference signal. The number of averaged periods of the excited harmonic perturbations was varied from 40 for 0.5 Hz to 120 for 20 Hz frequency. The sampling frequency was set in a way to provide about 40 points (always integer number) per fundamental period. The ensemble averaged signals were subjected to discrete Fourier transform to obtain mean amplitude and phase of disturbances at the excitation frequency f_1, as well as at frequency of its harmonic $f_2 = 2f_1$ to control a degree of nonlinear distortion of the disturbances. The mean-flow velocity was measured during about 10–15 s in every spatial position.

3. Theoretical approaches

This section is focused upon theoretical approaches used in the present study to describe unsteady Görtler vortices. The disturbance velocity–vector components corresponding to the coordinate-system axes described above and pressure are: $u(x, y, z, t)$, $v(x, y, z, t)$, $w(x, y, z, t)$, and $p(x, y, z, t)$, while mean-velocity-vector components are designated as $U(x, y)$, $V(x, y)$ and $W \equiv 0$.

To be consistent with previous theoretical studies, all these variables are made non-dimensional in this section using the so-called boundary layer scaling, which differs from the experimental ones in using Reynolds number $Re_0 = \sqrt{U_0 x_0/\nu}$ instead of local one Re^*. We assume that the excitation of disturbances occurs locally at $x = x_0 > 0$ from inside the boundary layer, therefore x is scaled by x_0, and the streamwise velocities U and u are normalized with respect to the free-stream velocity U_0 at x_0. The wall-normal and spanwise coordinates y and z as well as the wall radius of curvature are made dimensionless with respect to x_0/Re_0, while the wall-normal and spanwise velocities V, v, and w are scaled with U_0/Re_0. The pressure is scaled with $\rho U_0^2/Re_0^2$ and time t is scaled with x_0/U_0.

Let us consider stability of a two-dimensional *nearly* Blasius boundary layer over a concave wall of radius of curvature $R \gg 1$ at high-Reynolds number limit. In this case the Navier–Stokes equations linearized about the two-dimensional, steady base flow (U, V, 0) are reduced to [17,18]

$$
\begin{aligned}
&u_x + v_y + w_z = 0,\\
&u_t + Uu_x + U_x u + Vu_y + U_y v = u_{yy} + u_{zz},\\
&v_t + Uv_x + V_x u + Vv_y + V_y v + 2G\ddot{o}^2 Uu + p_y = v_{yy} + v_{zz},\\
&w_t + Uw_x + Vw_y + p_z = w_{yy} + w_{zz}.
\end{aligned}
$$

These equations are parabolic and, consequently, require initial conditions at x_0 and appropriate boundary conditions ($u = v = w = 0$) at the wall and in the free stream.

Since the mean-flow is assumed to be independent of spanwise direction, it is possible to consider solutions periodic in z with a spanwise wavenumber $\beta = 2\pi/\lambda_z$ and assume solutions of the form

$$
\begin{aligned}
(u, v, w, p) = \{&u(x, y, t)\cos\beta z, v(x, y, t)\cos\beta z, w(x,\ y,\ t)\\
&\sin\beta z, p(x,\ y,\ t)\cos\beta z\}.
\end{aligned}
\tag{1}
$$

Let us suppose also that the disturbances are harmonic in time and denote the dimensionless angular frequency (Strouhal number) of oscillations as $\omega = 2\pi f x_0/U_0$. After simple transformations this yields

$$\overline{u}_x + \overline{v}_y + \beta\overline{w} = 0, \tag{2}$$

$$(U\overline{u})_x + V\overline{u}_y + U_y\overline{v} = \overline{u}_{yy} - \beta^2\overline{u} + i\omega\overline{u}, \tag{3}$$

$$(U\overline{v} + V\overline{u})_x + 2(V\overline{v})_y + \beta V\overline{w} + 2G\ddot{o}^2 U\overline{u} + \overline{p}_y = \overline{v}_{yy} - \beta^2\overline{v} + i\omega\overline{v}, \tag{4}$$

$$(U\overline{w})_x + (V\overline{w})_y - \beta\overline{p} = \overline{w}_{yy} - \beta^2\overline{w} + i\omega\overline{w}, \tag{5}$$

the conservative form of the equations being convenient for their numerical solution by marching [27]. At $G\ddot{o} = 0$ this set of equations is also equivalent to that used by Luchini [28] in studying the optimal disturbances in flat-plate boundary layer and at $\omega = 0$ to that used by Hall [21] in studying the development of stationary Görtler vortices in growing boundary layer. We will call these equations throughout the text as linear *non-parallel stability equations* (NSE).

When $G\ddot{o} \lesssim \mathcal{O}(1)$ and $\beta \lesssim \mathcal{O}(1)$, it had been established [20] that the normal-mode approach is not acceptable, at least for stationary modes. At larger values of $G\ddot{o}$ and β the problem can be further reduced to a set of ordinary differential equations by factorizing $\overline{f}(x, y) = \widehat{f}(y)\exp(i\alpha x)$, where $\overline{f}$ is any of $\overline{u}, \overline{v}, \overline{w}$ or $\overline{p}$ and α is a local complex-number streamwise wavenumber. This yields a quasi-parallel approach similar to that used in [19] for the steady vortices

$$i\alpha\widehat{u} + \widehat{v}_y + \beta\widehat{w} = 0, \tag{6}$$

$$U_x\widehat{u} + i\alpha U\widehat{u} + V\widehat{u}_y + U_y\widehat{v} = \widehat{u}_{yy} - \beta^2\widehat{u} + i\omega\widehat{u}, \tag{7}$$

$$i\alpha U\widehat{v} + V_x\widehat{u} + V\widehat{v}_y + V_y\widehat{v} + 2G\ddot{o}^2 U\widehat{u} + \widehat{p}_y = \widehat{v}_{yy} - \beta^2\widehat{v} + i\omega\widehat{v}, \tag{8}$$

$$i\alpha U\widehat{w} + V\widehat{w}_y - \beta\widehat{p} = \widehat{w}_{yy} - \beta^2\widehat{w} + i\omega\widehat{w}. \tag{9}$$

If β, ω, $G\ddot{o}$, $U(x, y)$ and $V(x, y)$ are given, the equations constitute the eigenvalue problem in α. We denote these equations as linear *locally non-parallel stability equations* (LNSE).

The equations can be reduced even more by neglecting V and the streamwise derivatives of the mean velocities (i.e. assuming local parallelism of the flow streamlines) yielding

$$i\alpha\widehat{u} + \widehat{v}_y + \beta\widehat{w} = 0, \tag{10}$$

$$i\alpha U\widehat{u} + U_y\widehat{v} = \widehat{u}_{yy} - \beta^2\widehat{u} + i\omega\widehat{u}, \tag{11}$$

$$i\alpha U\widehat{v} + 2G\ddot{o}^2 U\widehat{u} + \widehat{p}_y = \widehat{v}_{yy} - \beta^2\widehat{v} + i\omega\widehat{v}, \tag{12}$$

$$i\alpha U\widehat{w} - \beta\widehat{p} = \widehat{w}_{yy} - \beta^2\widehat{w} + i\omega\widehat{w}. \tag{13}$$

This approximation is close in essence to that used by Görtler [7] with the exception that he considered the temporal formulation of instability to zero-frequency disturbances and, consequently, assumed ω purely imaginary and put $\alpha = 0$. This set of equations will be denoted as linear *locally-parallel stability equations* (LPSE).

Due to the long-standing question on the borders of applicability of different approaches in respect to β and $G\ddot{o}$ to describe accurately the development of steady Görtler vortices, we found it particularly important to compare the capabilities of the limit cases (i.e. LPSE and NSE) to predict the characteristics of the experimentally observed quasi-steady and unsteady Görtler vortices in the most problematic (and most important, simultaneously) region around $\beta = \mathcal{O}(1)$. The LNSE (and their generalization with kept p_x/Re^2 term) were used mainly in building isocontours of neutral stability and amplification rates and to ensure that the used numerical schemes (described below) provide the same results at the limit case of $\omega = 0$ as those obtained in previous studies devoted to the stationary Görtler-vortex instability.

To solve eqs. (14)–(17) and (10)–(13) we used a pseudospectral approximation of velocity derivatives $\partial/\partial y$ and $\partial^2/\partial y^2$ by Chebychev polynomials in N Gauss–Lobatto points [42,43]. A rational coordinate transform

$$y = a\frac{1+\xi}{b-\xi},$$

where a and b are adjustable parameters, mapped the problem from the polynomial domain $\xi \in [-1;\ +1]$ to the physical domain $[0; y_{\max}]$ along y. Value $y_{\max} = 2a/(b-1)$ was taken far away from the boundary-layer edge (here we present results obtained with $y_{\max} = 44$, $b = 2$ and $N = 70$). The solutions of the resulting discrete eigenvalue problems were obtained with standard technique utilizing the QZ-algorithm [44]. To march the parabolic eqs. (2)–(5) in the x-direction we used procedures equivalent to those described in [27]. The number of steps in x-directions $M = 200$ was used in the calculations. Both coding and computations were performed in MATLAB. Integration starts, if another is not specified, at $G\ddot{o}^* = 3.00$. (Note, that in the experiment the disturbances were excited at $G\ddot{o}^* \approx 7.16$.) Since the main emphasis of the calculations was to perform comparisons with the experimental data, the numerical results were renormalized for presentation in this paper to match the experimental scaling.

Solutions of eqs. (10)–(13) at x_0 were used mostly as the initial conditions in solving eqs. (2)–(5) in the paper. Dependence of the solution on the initial conditions is discussed in Section 6.1.

4. Base-flow characteristics

It was found that the potential-flow characteristics over the experimental model were independent practically of the spanwise coordinate z and the incoming flow velocity at least in the range between 3 and 15 m/s. The main measurements were carried out at free-stream velocity $U_0 = 9.18$ m/s.

By means of adjustment of the wall-bump shape (located above the experimental model, Fig. 1) an almost zero-gradient streamwise distribution of the potential-flow velocity was realized in the experiments. A special procedure of correction of the mean-velocity measurements was applied in order to detect even very small streamwise velocity gradients remaining possibly in the flow. (This procedure provided renormalization of the mean-velocity values measured with the hot-wire by the incident flow velocity measured permanently at the wind-tunnel test-section inlet.) The results have shown that an extremely weak favorable streamwise velocity gradient (of about 1% per meter) was still present in the potential flow in the range between $x = 400$ and 900 mm. Note, however, that so weak gradient did not influence, in fact, the linear Görtler instability characteristics (as was shown in special calculations).

Three typical wall-normal profiles of the streamwise mean-velocity component $U(y)$ measured inside the boundary layer are given in Fig. 4a in comparison with the Blasius profile. The experimental profiles are taken in the beginning, in the middle and in the end of the region of main measurements. Here and hereafter the streamwise velocities are normalized by the boundary-layer edge velocity U_e, while the wall-normal coordinate y is scaled with the local boundary-layer displacement thickness δ^*. It is seen that the distinction between the measured and calculated profiles is practically indistinguishable. However, more accurate comparisons performed for streamwise distributions of integral boundary-layer parameters: displacement thickness δ^*, momentum thickness δ^{**}, and the shape factor $H = \delta^*/\delta^{**}$, display clearly the presence of the weak favorable pressure gradient found during potential-flow measurements and indicated above (Fig. 4b). This gradient leads to a slight reduction after $x = 400$ mm of the boundary-layer thickness growth and to a small drop of the shape factor in comparison with the zero-gradient (Blasius) flow.

Since the physical nature of the steady Görtler instability is inviscid [1], the dependence of its characteristics on small variations of mean-velocity profiles is expected to be also weak for quasi-steady vortices. However, as indicated above, at high frequencies the regions of the Görtler and Tollmien–Schlichting instabilities approach each other [33], and the viscosity can play

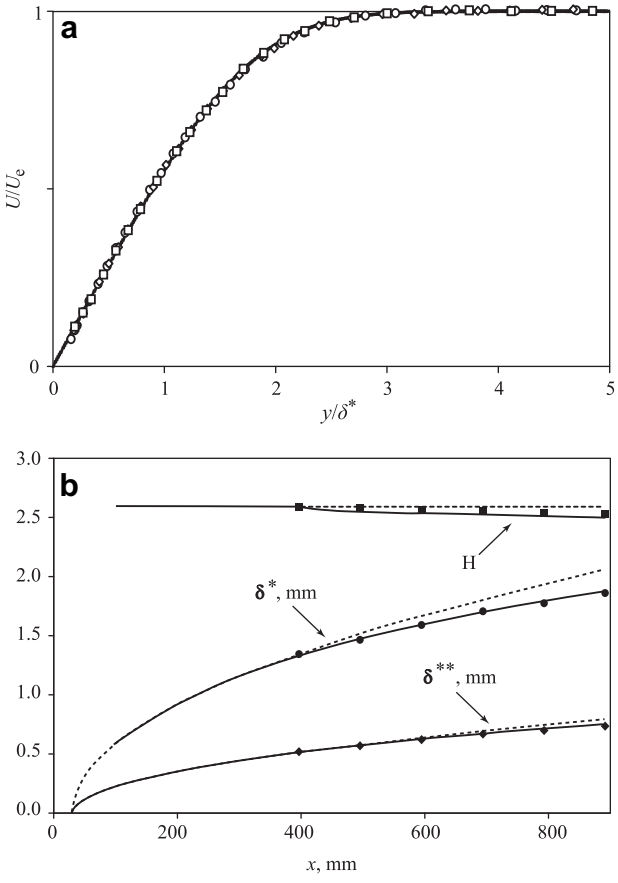

Fig. 4. Comparison of measured (at $z = 0$) and calculated wall-normal mean-velocity profiles: Blasius profile (−); $x = 397$ (□), 694 (◇), and 892 mm (○) (a) and downstream evolution of integral boundary-layer parameters measured (symbols) and calculated for Blasius (dashed lines) and for experimental conditions (solid lines) (b).

a certain role in the development of 'high-frequency' Görtler modes. Moreover, even small pressure gradients and mean velocity deformations are able to influence development of TS-waves [45]. Hence, a more rigorous approach used in the present investigation consists in the boundary-layer calculation using two-dimensional Prandtl equations in the so-called inverse-mode, when experimental data for δ^* were used as the free-stream boundary conditions [46].

To solve the Prandtl boundary layer equations in the inverse-mode, Crank–Nicolson implicit scheme with simple iterative update of coefficients [47] was used. Velocity profile of self-similar Blasius boundary layer was used as the initial condition applied at x_0. The same knots in y and x-directions were used as described in Section. 3. It is seen in Fig. 4b, that the numerical approximation provides the required correspondence of values and laws of evolution of all three generally used integral boundary-layer parameters throughout the measurement region.

In order to exclude any possible, in principle, influence of uncontrolled steady Görtler vortices (which might be generated by weak surface waviness), some special measurements of the spanwise non-uniformities of the base-flow structure were performed in the most downstream measurement location $x = 892$ mm in regimes without excitation of controlled perturbations. These measurements have shown that the uncontrolled Görtler vortices have very low (immeasurable, in fact) amplitudes, which do not exceed 0.1% of U_e and should not influence the development of the controlled disturbances excited by the source.

5. Regimes of measurements and spectral content of excited perturbations

In order to analyze the Görtler-instability problem and to perform comparison of experimental and numerical results correctly, it is necessary to know the complete set of all possible instability modes under the experimental conditions, to carry out their identification, and to take into account the disturbance-source near-field. All these points were analyzed and accounted for during selection of experimental regimes of excitation, subsequent measurements, and data processing.

The detailed measurements were carried out in 22 different regimes of disturbance excitation for eight frequencies of Görtler vortices and three values of spanwise wavenumber. The Görtler number $G\ddot{o}^*$ grew in the streamwise direction within the region of measurements between 10.3 ± 0.1 and 17.3 ± 0.1 (x = 397–892 mm). The values of the dimensional spanwise wavelength were $\lambda_z = 8$, 12, and 24 mm and corresponded approximately to the range of most dangerous wavenumbers. Note, that the corresponding dimensionless spanwise wavenumbers scaled with local boundary-layer displacement thicknesses changed downstream and constituted $\beta = 2\pi\delta^*/\lambda_z = 1.06$–$1.46$, 0.70–0.97, and 0.35–0.49, respectively. The spanwise wavelengths were taken to be small ($\lambda_z = 8$ mm), quite similar (12 mm) and large (24 mm) compared with the boundary-layer thickness ($\sim 3\delta^*$) inside the region of measurements that could be significant in sense of the Hall's criterium of applicability of the local analysis [27,28].

Because of the streamwise variation of β, the dimensionless spanwise wavelength parameter defined as

$$\Lambda = (U_0\lambda_z/\nu)(\lambda_z/R)^{1/2}$$

is used frequently in local analysis. That is $\Lambda = 149$, 274, and 775 for the given λ_z, respectively.

The stability diagram in the ($G\ddot{o}^*$,Λ)-plane calculated by means of LNSE for stationary Görtler vortices developing in Blasius boundary layer is shown in Fig. 5. Both the neutral stability curve

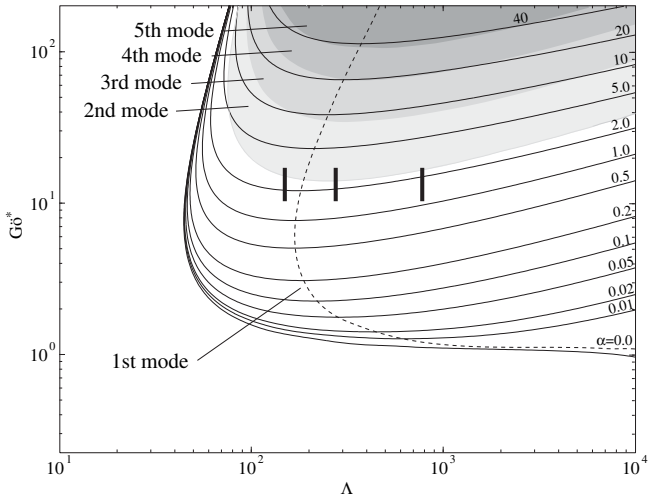

Fig. 5. Location of regions of measurements (thick vertical lines) on the stability diagram for steady Görtler vortices. Shaded areas show instability regions for higher modes. Dotted curve indicates the line of maximum growth for the first mode.

(i.e. the curve corresponded to amplification rate $(-\alpha_i) = 0$) for the first and higher discrete-spectrum instability modes and the contours of growth rates of the first discrete-spectrum Görtler mode are shown. The locations of all curves obtained for the first mode coincide perfectly with those given in Ref. [19,48]. Note, however, that the location of lower branch of the neutral stability curve cannot be justified for most value of Λ, as it has been shown with the help of asymptotic theory [21]. Later computations in Ref. [49] for $\Lambda \leq 210$ and in Ref. [24] for $\Lambda \leq 445$ determined more exactly that vortices show local growth rates independent of initial conditions and close to those obtained from local theories only at $G\ddot{o}^* \gtrsim 10.5$.

It is seen in Fig. 5 that the disturbance parameters were selected in experiment in a way to provide: (*i*) a moderate growth of vortices to avoid amplification of uncontrolled disturbances and their influence on the controlled ones, (*ii*) a closeness to the line of the most rapidly growing steady Görtler vortices, and (*iii*) an independence of the vortex growth from the initial conditions at least in a part of the $\Lambda - G\ddot{o}^*$ -region covered experimentally.

Moreover, the selected disturbance parameters correspond to the vicinity of the instability domain found for the first mode of *essentially unsteady* Görtler vortices up to the highest measured frequency of 20 Hz (see Section 8.2). The experiments were performed at frequencies $f = 0.5$ (for $\Lambda = 274$ only), 2, 5, 8, 11, 14, 17, and 20 Hz. The corresponding inviscid dimensionless frequency parameter $\omega = 2\pi f x_0/U_0$ (introduced in Section 3 and corresponded to Strouhal number) depends on the choice of x_0 and, therefore, is somewhat inconvenient for presentation of the experimental data (for which local scalings are accepted). In the corresponding viscous problem of the Tollmien–Schlichting instability of the Blasius boundary layer an independent of x dimensionless frequency parameter defined as

$$F = 2\pi f\nu/U_0^2 \times 10^6$$

is widespread. We found that it is quite convenient to use this parameter in the present study as well. The studied dimensional disturbance frequencies indicated above correspond to the frequency parameters $F = 0.57 \pm 0.01$, 2.27 ± 0.04, 5.67 ± 0.09, 9.08 ± 0.14, 12.48 ± 0.20, 15.89 ± 0.25, 19.29 ± 0.31, and 22.70 ± 0.36. The uncertainties are associated with variation of the air kinematic viscosity during the experiments.

Three examples of the unsteady Görtler-mode eigen spectrum presented in Fig. 6 are calculated based on eqs. (10)–(13) for $G\ddot{o}^* = 17.3$, $\Lambda = 149$ at three different frequencies corresponding to the lowest, moderate, and highest ones studied experimentally. The spectra demonstrate the combination of discrete eigenvalues and a discrete numerical approximation of the continuous branch. The content of the continuous-spectrum varies depending on the location and number of the selected knots. In contrast, the discrete-spectrum eigenvalues keep their position on the complex plane, if N and y_{max} are sufficiently large as in the present case, when $N = 70$ and $y_{max} = 44$.

The subsets of the spectra displayed in Fig. 6 contain also two discrete modes each. At $F = 0.57$ the two modes are amplified, at $F = 9.08$ only the leading (first) mode grows, while at $F = 22.70$ the two modes decay at given $G\ddot{o}^*$ corresponding to the last streamwise position of the measurements. Although the discrete modes are well separated from the continuous branch at the first two frequencies, in the last case the decay rate of the leading (first) discrete mode is very close to that of the continuous-spectrum tip (at $\alpha_i \approx \beta^2$). This implies that the first discrete Görtler mode can be easily identified experimentally at $G\ddot{o}^* = 17.3$ at the first and the second frequency, while at the third one such identification might be difficult and an extensive near-field region behind a disturbance source is expected. Note, however, that since we are interested mainly in the *most rapidly amplified* Görtler-instability disturbances (which correspond to the first discrete mode) the cases like the third one in Fig. 6 are interesting basically in finding limitations of the experimental and numerical approaches used.

Although under the present experimental conditions the second discrete Görtler-instability mode starts to grow slowly in the very end of the region of measurements (at very low frequencies only) it does not play any significant role in the disturbance development in all studied cases (see Section 6.2 and, especially, Ref. [50]). Higher discrete-spectrum modes turned out to be always attenuating at the present experimental conditions.

6. Spatial shapes of quasi-steady and unsteady Görtler vortices

6.1. Wall-normal profiles of Görtler vortices. Predominance of the first mode in experiment

The analysis of the instability-mode eigenfunctions provides the most reliable way of the instability-mode identification. It is well-known that the first Görtler mode with *zero frequency* consists of only one vortex layer in the wall-normal direction and has one amplitude maximum, while the higher discrete-spectrum modes (second, third, *etc.*) have two, three, and more counter-rotating vortex layers and amplitude maxima [51].

The present study has shown that the *amplitude parts* of eigenfunctions of the *unsteady* Görtler modes are similar to those of steady ones. An example is presented in Fig. 7(left) for the first and the second unsteady discrete-spectrum Görtler-instability modes. The disturbance maximum of the first mode is close to the critical layer, where the local mean-flow velocity is equal to the Görtler mode phase velocity (a circle in Fig. 7). The first-mode phase (right plot) decreases with the wall-normal coordinate in a linear way and differs significantly from the second-mode phase profile, which has a jump (about 180°) at the amplitude minimum located between two humps.

The third amplitude profile shown in Fig. 7(left) (dash-dotted line) displays function $y\partial U/\partial y$, which corresponds approximately to the so-called transient disturbances [28]. The shape of this profile is also different from those of the Görtler modes.

In general, the amplitude distributions of both the higher discrete-spectrum modes and the transients have relatively large amplitudes near the boundary-layer edge, while the first discrete-spectrum Görtler mode have almost zero amplitude there. Therefore, any admixture of the former to the first mode has to lead, first of all, to a distortion of the amplitude profile near the boundary-layer edge. This criterion was used extensively in the present work during identification of the first Görtler mode described below.

The dependence of the disturbance wall-normal profiles on the streamwise coordinate (and Görtler number $G\ddot{o}^*$), frequency parameter F, and spanwise wavelength parameter Λ is illustrated in Figs. 8–10 (for some of studied regimes) and discussed in the text. Symbols indicate experimental amplitude and phase distributions; dashed and solid lines show the profiles obtained numerically based on LPSE (for the first Görtler mode) and NSE (with initial conditions corresponding also to the first Görtler mode), respectively.

Typical downstream evolution of the experimental and theoretical profiles of disturbance phases (counted from the wall) φ_n and amplitudes A_n (normalized by their maximum values) is shown in Fig. 8 for $F = 5.67$ and $\Lambda = 149$. It is seen that in the end and in the middle of the studied streamwise region (starting with $x = 595$ mm) the agreement between the measured and calculated profiles is very good. However, close to the disturbance source (at $x = 397$ and 496 mm) the experimental amplitude points

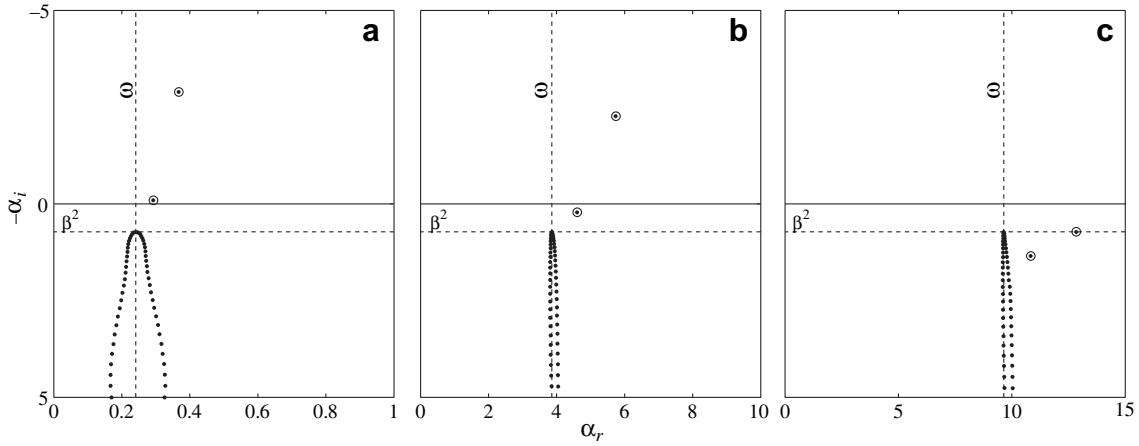

Fig. 6. Spectra of eigenmodes for unsteady Görtler vortices based on eqs. (10)–(13) with Blasius mean-velocity profile calculated for $G\ddot{o}^* = 17.3$, $\Lambda = 149$ at $F = 0.57$ (a), 9.08 (b), and 22.70 (c): discrete modes (○); numerical representation of continuous modes (●;); lines $\alpha_r = \omega$ and $\alpha_i = \beta^2$ (----).

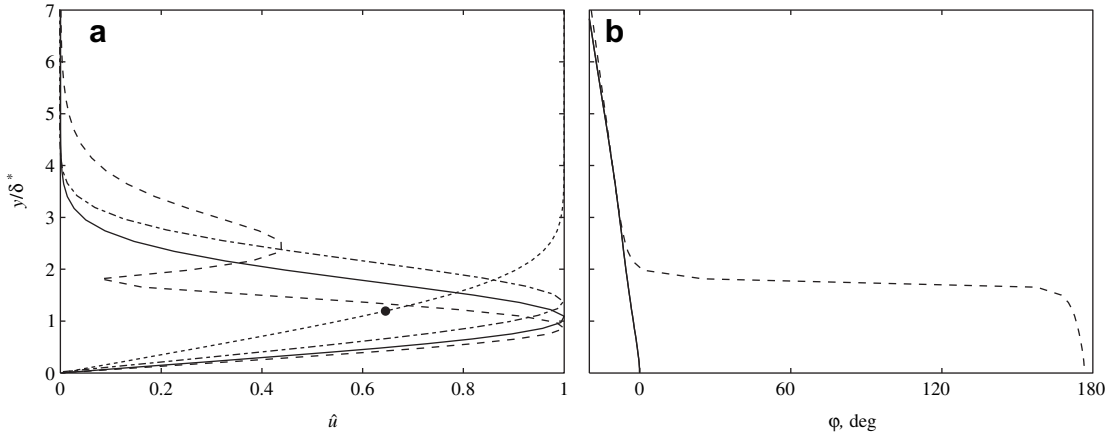

Fig. 7. Amplitude (a) and phase (b) profiles of two most amplified discrete-spectrum modes of unsteady Görtler-instability problem calculated by means of LPSE at $\Lambda = 149$, $F = 0.57$, $G\ddot{o}^* = 17.3$. (–), first mode; (- - -), second-mode; (···), mean velocity; (– · –), ydU/dy; (●), location of critical layer for the first mode.

deviate from the calculated profiles. This discrepancy can be explained by the presence in the disturbance-source near-field of attenuating transient disturbances excited in the boundary layer along with the amplified discrete Görtler mode. As x grows, the transients attenuate, the second potentially unstable Görtler mode lags in amplification (or attenuates), as expected, and the most amplified first Görtler mode becomes predominant at $x \gtrsim 600$ mm ($G\ddot{o}^* \gtrsim 13.2$) providing the agreement of the experimental and numerical profiles. The numerical profiles obtained with NSE and LPSE are quite similar. The agreement between the experimental profiles and those calculated by means of the LPSE-approach indicates that the measured disturbances correspond to the first Görtler mode in the disturbance-source far-field. However, the NSE-approach provides slightly better agreement with the measurements in the source far-field. Note also, that when the disturbance propagates downstream, its amplitude maximum shifts slightly towards the wall, while the phase slope slightly increases. These trends are equally observed in both the experimental and theoretical profiles.

Typical frequency dependence of the wall-normal amplitude and phase profiles in the disturbance source far-field is illustrated in Fig. 9 for $x = 892$ mm ($G\ddot{o}^* = 17.3$), $\Lambda = 274$. As the frequency increases, the disturbance amplitude maximum is displaced a little away from the wall without any significant change of the profile shape. This is equally observed in the experiment and in the two calculations and differs from the known behavior of transient disturbances occurred in the flat-plate boundary layer, the amplitude maximum of which is always located near $y/\delta^* \approx 1.5$ for $F \approx 18.5$–35.0 and the corresponding amplitude profiles are characterized by appearance of a small-amplitude region near the wall [52,53], which is not seen in the present case.

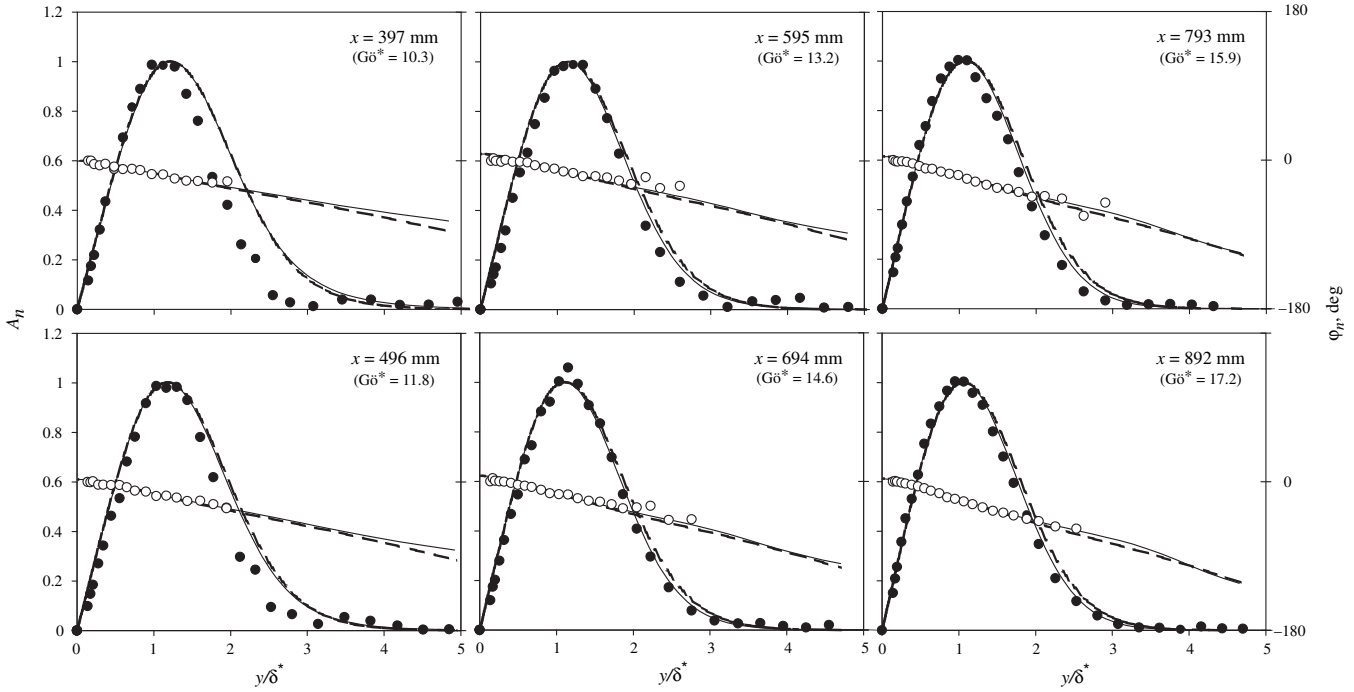

Fig. 8. Downstream evolution of experimental amplitude (●) and phase (○) profiles of boundary-layer disturbances in comparison with those calculated by NSE (–) and LPSE (- - -) for the first Görtler mode. $F = 5.67$, $\Lambda = 149$.

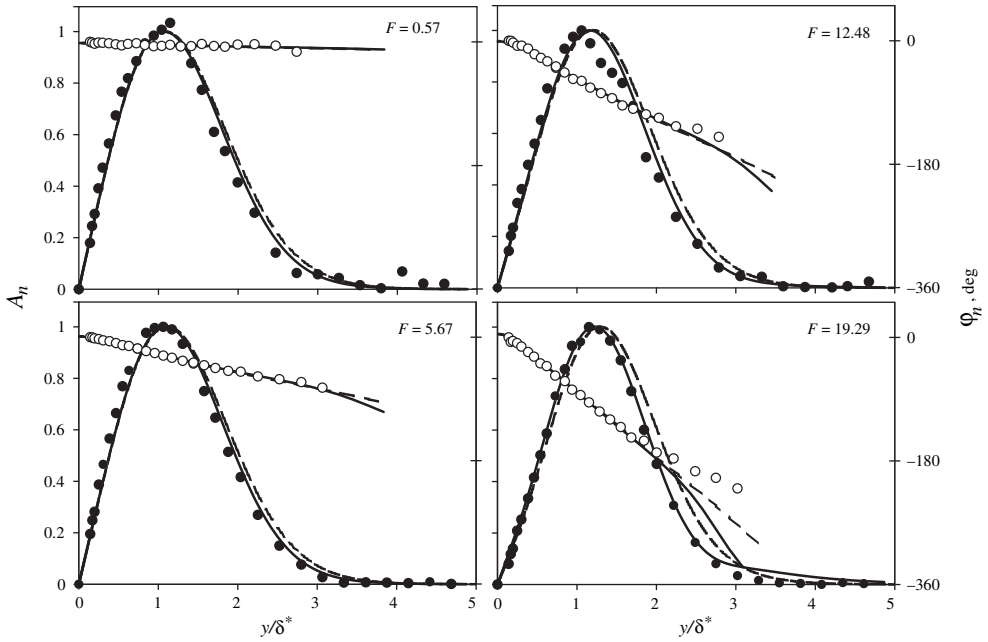

Fig. 9. Illustration of frequency dependence of amplitude and phase profiles of boundary-layer disturbances measured and calculated for the first Görtler mode in the source far-field (at $x = 892$ mm). $\Lambda = 274$, $G\ddot{o}^* = 17.3$. (See Fig. 8 for legend.).

A strong frequency dependence is observed for the disturbance phase profiles, whose nearly linear tilting along y-coordinate increases substantially with frequency. At high frequencies this dependence results in very large phase delays between the near-wall region and the outer layer. At $F \gtrsim 19.29$ this delay reaches and exceeds 180°, i.e. the vortical motions near and far-from the wall occurs with opposite phases. This corresponds to formation of a specific spatial structure of unsteady Görtler vortices described below in Section 6.2.

The measured amplitude and phase profiles and those calculated with the NSE and LPSE shown in Fig. 9 are in a good agreement for all frequencies. At high frequencies the NSE-approach displays a somewhat better agreement with the experiment for the amplitude profiles.

All aforesaid comments (related to the cases with $\Lambda = 274$) are valid for the disturbance amplitude and phase profiles obtained for $\Lambda = 149$ (in the whole studied frequency range) and $\Lambda = 775$ (in the frequency range of *amplified* vortices of the first Görtler mode, i.e. for $F \leq 9.08$). However, the situation is different for *weakly* amplified or *attenuating* first-mode disturbances (see Fig. 10). The total perturbations can be interpreted in this case as a mixture of the first-mode Görtler vortices and the transients, whose relative amplitudes remain comparable to each other for a long downstream distance. This point is able to influence both the results of NSE-calculations and the measurements. When the first Görtler mode has nearly neutral behavior or attenuates (weaker usually than all continuous-spectrum modes) it does not have enough streamwise distance to become predominant even up to the last studied section with $x = 892$ mm ($G\ddot{o}^* = 17.3$), despite the disturbance source in the experiment is still located far upstream (at $x = 207$ mm; $G\ddot{o}^* = 5.97$) and the integration in the NSE-approach still starts at $x = 100$ mm ($G\ddot{o}^* = 3.00$). This problem can be solved providing more suitable initial conditions with smaller content of transient disturbances, consequently, favoring the first Görtler mode from the very beginning.

When the first Görtler mode attenuates faster than the leading continuous-spectrum modes or even has the same attenuating rate (see, e.g., Fig. 6c), the former has no chance to become dominant

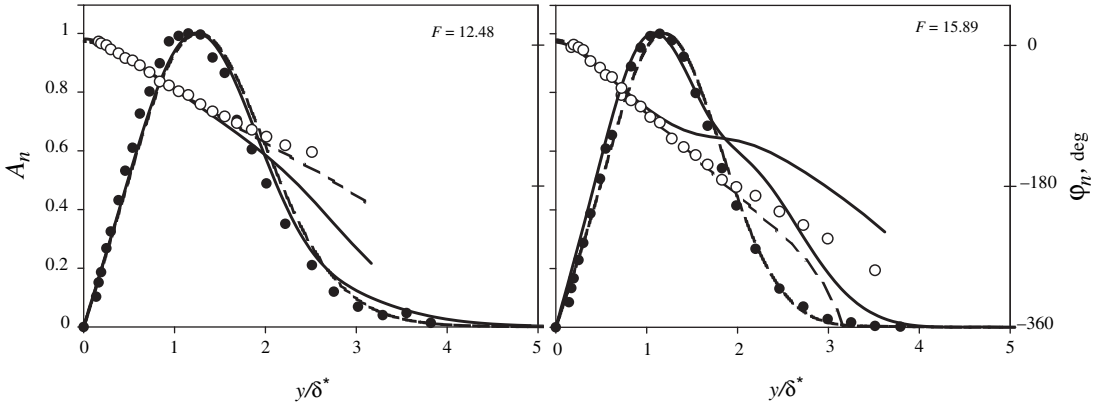

Fig. 10. Wall-normal profiles of disturbance amplitudes and phases measured and calculated for the weakly amplified or attenuated first mode of unsteady Görtler instability. $\Lambda = 775$, $G\ddot{o}^* = 17.3$. (See Fig. 8 for legend.).

until (and if) the flow becomes less stable to it, as $G\ddot{o}^*$ increases. In such a case a displacement of the initial location x_0 downstream could provide better conditions for studying the first mode both in experiment and in the NSE-approach. Therefore, the NSE-profiles shown in Fig. 10 were calculated for initial conditions applied at $G\ddot{o}^* = 10.3$ (instead of usual $G\ddot{o}^* = 3.00$), i.e. in the beginning of the region of measurements. This modification helped to solve the problem at $F = 12.48$. However, even in this case some distortions are visible on the NSE-amplitude profiles at frequency $F = 15.89$ (and higher, not shown). The NSE-phase profiles deviate also from both the experimental ones and from those calculated by means of the LPSE. In this specific group of regimes (with weakly amplified or attenuated first-mode Görtler vortices) the LPSE provides a better agreement with experiment than the NSE (usually vice versa) despite the former does not take into account the effects of the base-flow non-parallelism. Thus, even in these difficult cases the experimental disturbance source produces (in its far-field) the first discrete-spectrum Görtler mode basically.

It is found that there is a very little difference between the wall-normal amplitude and phase profiles studied for three different values of the spanwise wavenumber for the first-mode Götler vortices of constant frequency. This result supports the conclusion made above that the profile shapes are very conservative. Only a weak displacement of the amplitude maxima away from the wall is observed with growth of the vortex spanwise scale. The tilting of the phase distribution increases slightly as well both in the experiment and the calculations.

Thus, in spite of the complexities associated with accounting for the disturbance-source near-field in the NSE-calculations, the wall-normal profiles of the disturbance amplitudes and phases calculated for the first Görtler-instability mode are very close to those obtained experimentally for $G\ddot{o}^* \gtrsim 12$ for the growing perturbations (i.e. at $\Lambda = 149$ and 274, and for $F \leq 12.48$ at $\Lambda = 775$). Moreover, these profiles are in a good agreement with the corresponding eigenfunctions of the first unsteady Görtler mode obtained with the LPSE, which is free of the near-field problems by its definition. The NSE with the used initial conditions give somewhat better agreement with experiment in all cases *excluding* the case of attenuating or weakly amplifying vortices.

Hence, it is possible to conclude that the one and the same first Görtler-instability mode was measured experimentally and modeled theoretically. These results indicate also that the disturbance source used in the present experiments excites in the boundary layer (in a wide range of parameters) the disturbances, which represent essentially the most growing both quasi-steady and unsteady Görtler-instability modes.

6.2. Instantaneous shapes of quasi-steady and unsteady first-mode Görtler vortices

As far as the unsteady first-mode Görtler vortices has never been examined in previous studies, it was important to analyze their spatial shapes, which turned out to be quite different from those of the corresponding well-known steady vortices. Some results of this analysis are presented below.

Spatial shapes of the unsteady (in general) Görtler vortices are illustrated for the spanwise wavelength $\Lambda = 274$ in Fig. 11 for a quasi-steady case and in Fig. 12 for an essentially unsteady case. The instantaneous fields of the streamwise-velocity disturbance shown there are measured (plots *a*,*b*) and calculated (plots *c*) for the experimental conditions with the NSE-approach along with the calculated instantaneous vector fields of the velocity disturbance. The side views on the instantaneous fields measured in the (x, y)-plane and normalized at every x-coordinate by maximum value are shown in plots *a*. By means of this normalization the disturbance growth in the streamwise direction is neglected in order to highlight some peculiarities of the vortex shapes. The corresponding end views (the cross-sections by the (y, z)-plane) are shown in plots b and c.

Note that the reduction of the disturbance streamwise wavelength with frequency provides, in general, better conditions for validity of the locally-parallel (LPSE) approach. However, this statement is only partially true. Indeed, the wavelength reduction implies better conditions for the leading order solution, but this solution could be locally neutral and, in an asymptotic sense, the (higher order) growth rate could still be influenced by non-parallel effects, depending on the value of the Görtler number. It seems to us also that one should not neglect the effects of the base-flow non-parallelism even at the highest of studied frequencies (including $F = 22.70$) because even for much more high-frequency disturbances associated with strongly inclined TS-waves these effects are known to be important [54]. This importance is explained by very strong inclination angles of waves attributed to the unsteady Görtler vortices under study. Subsequent processing has shown that the wave propagation angles θ vary in the present experiment between 89.99 degree for the lowest studied frequency ($F = 0.57$) to 87.51 degree for the highest one ($F = 22.70$).

The experimental results presented in Fig. 11a, b illustrate a disturbance field typical for the first mode of steady Görtler vortices studied previously as streamwise elongated vortices with axes parallel to the wall. The pictures correspond to a time instant of a maximum instantaneous amplitude of the vortices. The negative velocity disturbance corresponds to rise of low-speed fluid from the near-wall region away from the wall, while the positive instantaneous velocity displays lowering of high-speed fluid towards the wall. The same behavior is seen in the numerical results presented in Fig. 11c. The instantaneous vector fields, shown there in addition, display one layer of counter-rotating (in the spanwise direction) streamwise elongated Görtler vortices. The intensity of rotation varies slowly with time and changes its sign after one half of period. The instantaneous shape of the quasi-steady vortices is independent practically of x, as seen in the (y, x)-plane (Fig. 11a). Thus, the results presented in Fig. 11 demonstrate that the experimental and theoretical spatial structure of quasi-steady first-mode Görtler vortices corresponds practically to that of the steady ones.

The situation observed for essentially unsteady Görtler vortices is different significantly (Fig. 12). In the cross-section (Fig. 12b and c) the structure consists of several cells associated with the strong dependence of the disturbance phase on the wall-normal coordinate observed at high frequencies (see Fig. 9) and leading to anti-phase oscillations of the streamwise velocity component at different distances from the wall. This phase behavior corresponds to a substantially different spatial shape of the vortices shown in Fig. 12 and results in an inclination of the unsteady first-mode Görtler vortices with respect to the wall (Fig. 12a). Due to this, several instantaneous counter-rotating vortex layers appears at different wall-normal distances in the cross-section view (Fig. 12c). In every fixed (y, x)-section the interface line between the vortex layers move towards the wall with time. The vortex amplitude increases initially with time (when the line is far-from the wall) and then decreases (when the line approaches the wall).

The angles of inclination of the Görtler vortex axes with respect to the wall, γ, were determined in the disturbance-source far-field based on results of numerical calculations performed within the framework of the NSE-approach. At $F = 0$ the inclination angle is equal to zero (as it should be), increases monotonously with frequency, and reaches 1.36° at $F = 22.70$, $\Lambda = 149$. The rate of increase of the angle grows with the spanwise wavelength Λ.

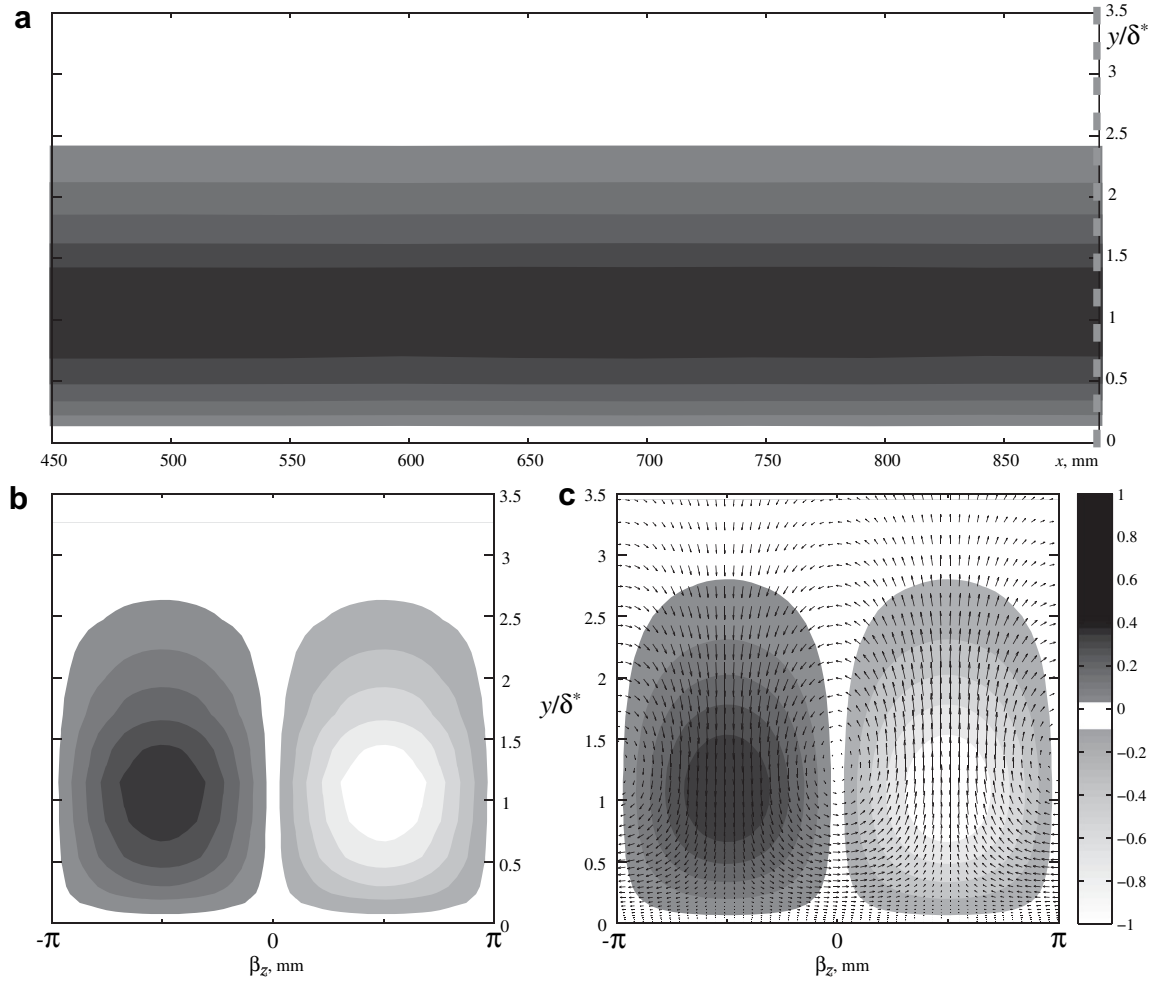

Fig. 11. Typical instantaneous shape of quasi-steady first-mode Görtler vortices. $F = 2.27$, $\Lambda = 274$. Plot (a): side view measured at $\beta z = \pi/2$. Plots (b, c): end view measured (b) and calculated (c) at $x = 892$ mm ($G\delta^* = 17.3$) marked at plot (a) with vertical dashed line. Shades of gray display levels of instantaneous streamwise-velocity disturbance. Arrows display projections of instantaneous vector fields of velocity disturbance onto the (y, z)-plane.

7. Evolution of Görtler vortices and linear-stability characteristics

7.1. Linearity of measured stability characteristics

In the present experiments a great attention was focused on the question of linearity of the stability problem under study, in particular to independence of properties and evolution characteristics of the studied Görtler vortices from their amplitudes. The tuning-out of the zero frequency and utilizing the new efficient disturbance source gave us the possibility to vary disturbance amplitudes in a wide range and to examine easily, in this way, some possible nonlinear effects.

Note, first of all, that the signal at the fundamental frequency of excitation was predominant in spectra of boundary-layer velocity perturbations. In particular, the uncontrolled ("natural") disturbances were much weaker in the studied frequency range. It was not found also any significant nonlinear generation of velocity fluctuations at frequencies of higher harmonics of the fundamental disturbance, as well as in the subharmonic frequency range.

The results presented in Fig. 13 were obtained at $\Lambda = 274$ in two tests of linearity performed for $F = 2.27$. In these tests the initial disturbance amplitudes used in the main measurements ($A_0 = 0.34\%$) were enhanced by a factor of two. The figures illustrate the experimentally established fact that the variation of initial amplitudes does not result in any change in laws of streamwise evolution of the Görtler vortices under study (Fig. 13, left), as well as in shape of the disturbance eigenfunctions (Fig. 13, right). This is consistent with some Hall's [22] and later numerical calculations. The mean-velocity profiles of the base flow do not display also any nonlinear distortions associated with presence of controlled Görtler vortices. Similar results were obtained in other regimes of disturbance excitation.

Thus, in the present experiment the characteristics of both the base flow and the disturbance evolution are independent of initial amplitudes at least up to 3.5% of U_e. Accordingly, all stability characteristics obtained in the present experiment do correspond to the characteristics of *linear* Görtler instability.

7.2. Estimations of range of applicability of modal analysis

Note that in the region of validity of the locally-parallel or locally non-parallel stability equations (LPSE or LNSE), the discrete-spectrum modes growing downstream correspond to Görtler vortices. Meanwhile in solving the non-parallel stability equations (NSE), as well as in experiment, the obtained disturbances are composed of large (infinite, in general) amount of modes, the most of which decay. Hence, the disturbance behavior close to a disturbance

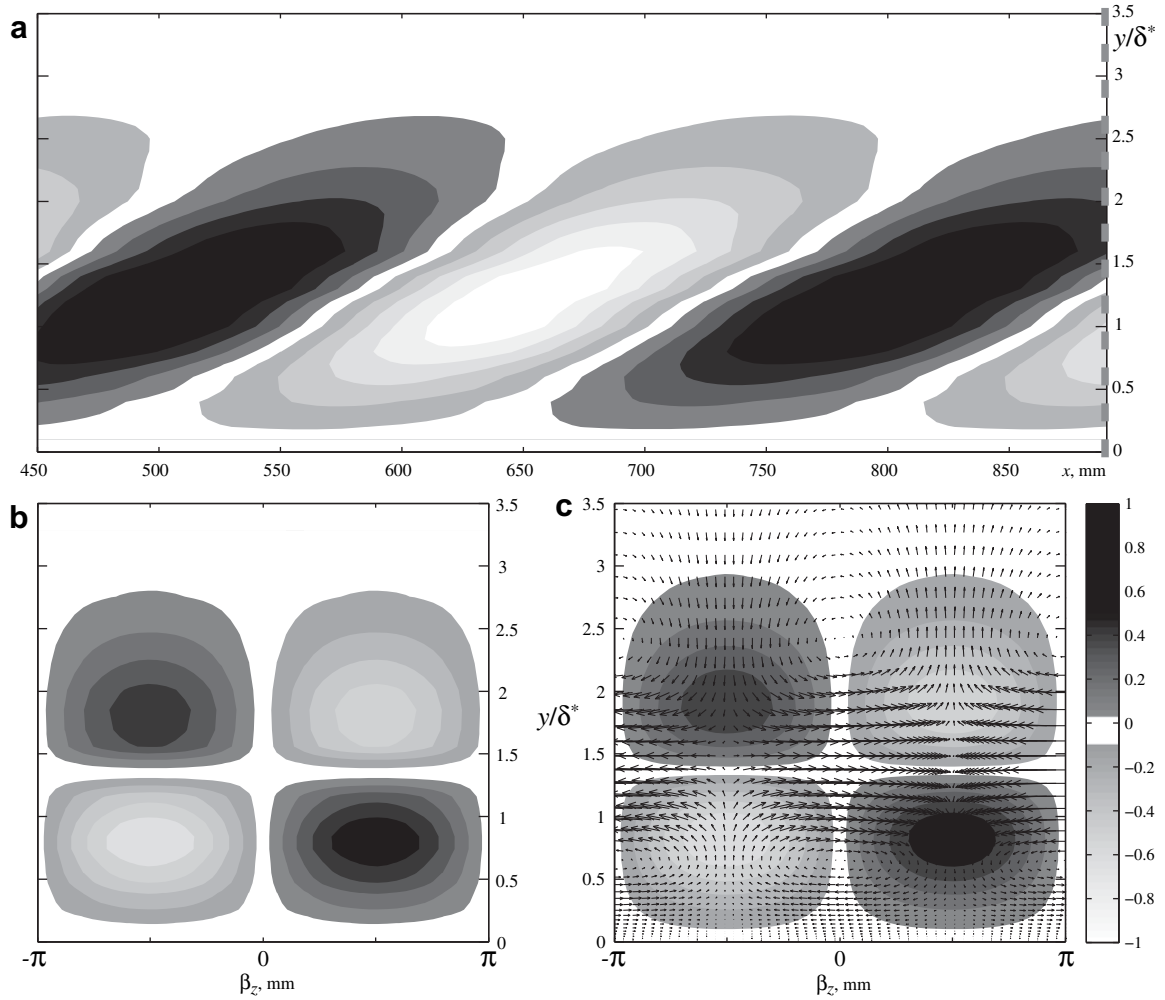

Fig. 12. Typical instantaneous shape of essentially unsteady first-mode Görtler vortices. $F = 22.70$, $\Lambda = 274$. Plot (a): side view measured at $\beta z = \pi/2$. Plots (b, c): end view measured (b) and calculated (c) at $x = 892$ mm ($G\ddot{o}^* = 17.3$) marked at plot (a) with vertical dashed line. Shades of gray display levels of instantaneous streamwise-velocity disturbance. Arrows display projections of instantaneous vector fields of velocity disturbance onto the (y, z)-plane.

source can be subjected to different transient effects behaving differently depending on initial conditions. In particular, a quite rapid transient growth of perturbations is possible there, as well as a rapid transient attenuation. Additionally, the inability of LPSE and LNSE to describe the instability at $\beta \gtrsim 1$ and small $G\ddot{o}^*$ [20,21] raises the question of permissibility of the modal approaches in the region of parameters studied in the present experiments.

To carry out an accurate comparison of theoretical, numerical, and experimental results in the near-field of the source at $G\ddot{o}^* \gtrsim 1$, it is required either to obtain complete solution of the corresponding receptivity problem or to perform detailed measurements of all disturbance velocity components at x_0 to provide the initial data for the governing equations. However, first, it is very difficult to measure very small wall-normal and spanwise velocity components (only streamwise component is measured in the present experiments) and, second, the receptivity problem is out of scope of the present study. Therefore, in the present case a set of some model velocity–disturbance profiles was used in order to approximate the required initial conditions and to estimate roughly the characteristic length of the disturbance-source near-field, i.e. the characteristic bound of the region, downstream of which the disturbance behavior would be expected free of the transient and non-modal effects. The procedure was found to be quite satisfactory for conditions of the present experiments in the whole range of experimental frequencies at $\Lambda = 149$ and 274 and for relatively low frequencies at $\Lambda = 775$ (as discussed in more detail in the next Section). This is in accordance with numerous previous theoretical and numerical findings that as soon as $\beta \gtrsim 1$ and $G\ddot{o}^*$ increases the Görtler vortices 'forget' peculiarities of initial conditions and approach the modal growth.

Several typical examples of such computations are shown in Fig. 14 along with the corresponding experimental data. The calculations were performed for some selected experimental parameters with the model initial conditions: $(a)\ \widehat{u}_0 = (1 - \cos y^2)\exp(-y^4/2), \widehat{v}_0 = \widehat{w}_0 = 0$, and $(b)\ \widehat{v}_0 = y^5\exp(-y^3), \widehat{u}_0 = \widehat{w}_0 = 0$, which were used previously at $\omega = 0$ in Ref. [21] for the same purpose. Shown there are amplification curves for the streamwise component of disturbance amplitudes $\hat{u}$ calculated and measured at wall-normal amplitude maxima and normalized by the value $\hat{u}_{\max}$ reached at $x = 892$ mm ($G\ddot{o}^* = 17.3$). Such normalization is convenient due to presence of different disturbance behavior in the disturbance-source near-field. The computations were started at $x = 200$ mm ($G\ddot{o}^* = 5.79$), i.e. close to the position of the experimental disturbance source. Results of calculations of the disturbance amplitude growth based on a local approach are also shown with solid lines for comparison.

It is seen that the bound predicted in such a way is located at $x \approx 500$–600 mm ($G\ddot{o}^* = 12.36$–14.28), i.e. 300–400 mm downstream the disturbance source. Based on these estimations the first

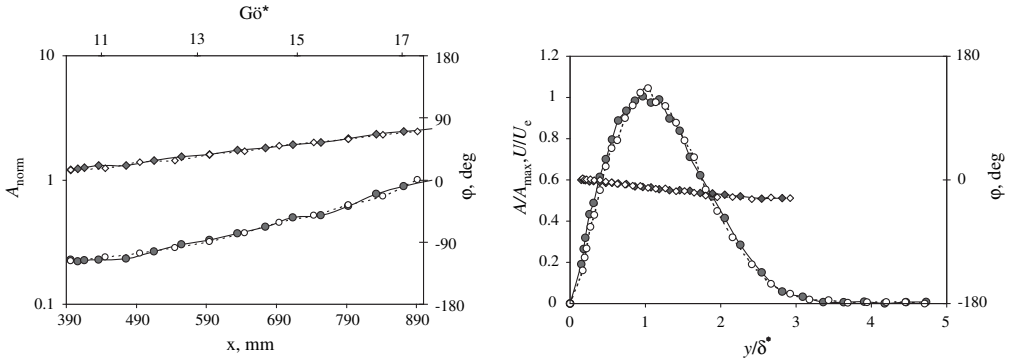

Fig. 13. Streamwise (left) and wall-normal (right) distributions of phases (diamonds) and normalized amplitudes (circles) of disturbances with $\Lambda = 274$ excited at $F = 2.27$ at initial amplitudes: $A_0 = 0.34\%$ (*filled symbols*); $2A_0 = 0.68\%$ (*open symbols*). Lines: approximations of experimental points.

measurement section was chosen at $x \approx 400$ mm ($G\ddot{o}^* = 10.33$). Subsequent measurements and calculations have shown (see Section 6.1) that the actual length of the near-field of the disturbance source corresponded, in general, to these estimations (as in Fig. 14).

7.3. Downstream evolution of disturbance amplitudes and phases

Streamwise distributions of the disturbance amplitudes and phases discussed below and presented in Figs. 15–18 are measured and calculated for wall-normal amplitude maxima of the streamwise component of velocity perturbations. The calculations were performed based on non-parallel stability equations (NSE) and locally-parallel stability equations (LPSE) described in Section 3. Filled symbols display experimental points corresponded to the disturbance-source far-field where the boundary-layer perturbations represent the first discrete-spectrum mode of Görtler instability (see Section 5). Open symbols display the results of measurements obtained within the disturbance-source near-field, where the disturbance, according to estimations, made above and in Section 6.1, represents a mixture of some transients and the first Görtler mode. Dashed lines display the LPSE-results, while solid lines correspond to calculations based on the NSE-approach. The disturbance amplification curves (Figs. 15 and 17) are presented in logarithmic scale. The *calculated* amplitude distributions are normalized by the values reached in the end of the region of measurements (i.e. at $x = 892$ mm, $G\ddot{o}^* \approx 17.3$), while all *calculated* phases are counted from values reached at the streamwise location of the first point of measurements (i.e. at $x = 397$ mm, $G\ddot{o}^* \approx 10.3$) The *experimental* amplitude and phase distributions are matched with the corresponding numerical ones calculated in the disturbance source far-field within the NSE-approach. In several cases when this approach gives incorrect results, which, hence, are not shown in the figures, the experimental distributions are matched with the LPSE-ones. Normalized in this way disturbance amplitudes are designated as A_{norm}. There are two abscissas in Figs. 15–18: (*i*) streamwise distance from the model leading edge (in mm), i.e. the *x*-axis, and (*ii*) the corresponding local Görtler number $G\ddot{o}^*$ indicated at the top of every plot.

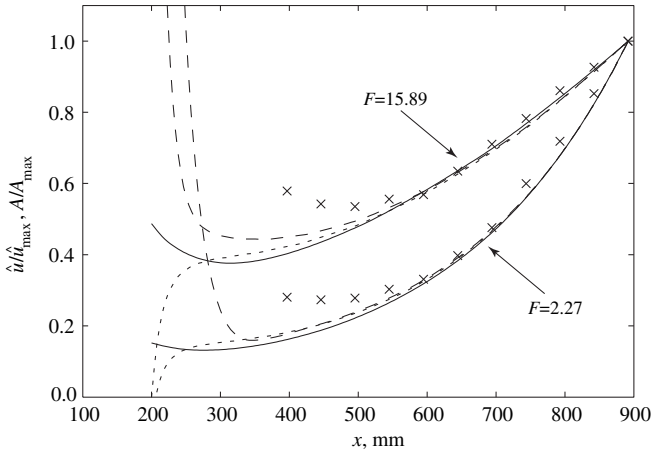

Fig. 14. Amplification curves of Görtler vortices calculated in the framework of LPSE-approach (solid lines) and NSE-approach (dashed lines) at different initial conditions, and measured (×) for $\Lambda = 149$ and $F = 2.27$ and 15.89. (—) normal-mode approach; (– –) and (- - -) are model initial conditions *a* and *b*, respectively.

Figs. 15–18 illustrate the overall excellent agreement between the experimental and theoretical results obtained in the present study in all studied regimes. In cases, when the first-mode Görtler vortices are amplified significantly, the NSE-results agree better with the experiment, than the LPSE-results. Meanwhile, in regimes with large spanwise wavelengths and high frequencies (i.e. at $\Lambda = 775$ and $F \geq 12.48$), where the first Görtler mode is either nearly neutral or attenuates, the situation is opposite: the LPSE agrees better, than the NSE, with the experiment. This observation is in agreement with the results of analysis of the disturbance wall-normal profiles and their comparison with Görtler-mode eigenfunctions presented in Section 6.1.

The regions where the experimental and theoretical results deviate from each other are relatively short at $\Lambda = 149$ and 274 and cover only first three or four experimental points on the amplification curves. This means that the first Görtler-instability mode becomes predominant in the experiment, as a rule, starting with $x \approx 500$–600 mm ($G\ddot{o}^* \approx 12$–13). As far as the NSE-calculations with different initial conditions also merge with the experimental points approximately in the same downstream section, it was accepted that the source near-field and/or the region of non-modal behavior ends in the point, where a good agreement of all experimental stability characteristics (including eigenfunctions, see Section 6.1) with the theoretical ones occurs.

The distributions obtained for the Görtler vortices with spanwise wavelength $\Lambda = 149$ (Figs. 15 and 16) show that both NSE and LPSE provide a very good, in general, agreement with experiment and can be used for the stability calculations and transition prediction. However, the amplitude and, especially, phase distributions calculated with the help of the NSE-approach agrees better with the measurements. In particular, a slightly better agreement of amplification curves is seen in the region close to the disturbance-source near-field (Fig. 15). This suggests, most probably, that the effects of the base-flow non-parallelism, which are not taken into

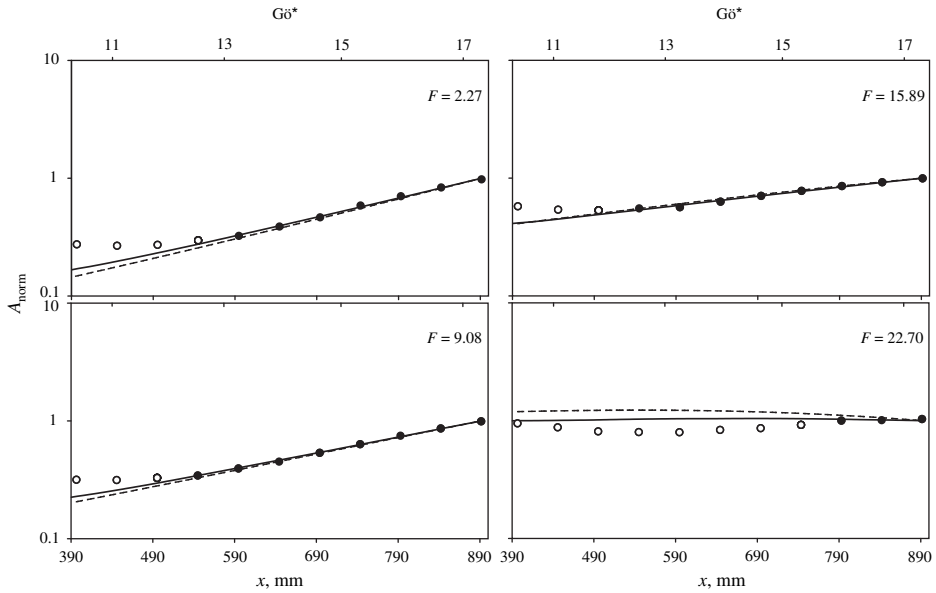

Fig. 15. Streamwise evolution of Görtler vortex amplitudes for $\Lambda = 149$ and various frequencies obtained experimentally (circles) and numerically by NSE (–) and LPSE (– – –): far-field (●); near-field (○).

account in the LPSE, are significant at $G\ddot{o}^* \lesssim 13$ similarly to steady vortices [20,21]. The rate of the disturbance amplitude growth decreases with frequency, while the disturbance phase growth increases. At high frequencies both calculations indicate that the flow becomes stable. The same is observed in the experiment despite the location of the experimental neutral point is somewhat different and the numerical decay is somewhat stronger.

For slowly growing and attenuating disturbances the NSE-approach also faces the difficulty of predominance of the first Görtler-instability mode (plot for $F = 22.7$ in Fig. 15). However, at the discussed spanwise wavelength ($\Lambda = 149$) this problem is not so significant, namely: (*i*) the measured wall-normal disturbance profiles coincide practically with eigenfunctions of the first Görtler mode even at high frequencies (Section 6.1); (*ii*) the amplification curves differ only marginally from the LPSE-results, which are free of the near-field effects by definition (Fig. 15); (*iii*) the measured phase distributions remain in a very good agreement with the calculations (Fig. 16).

The disturbance phase distributions measured and calculated for $\Lambda = 149$ (Fig. 16) display almost linear growth with the streamwise coordinate in both the experiment and the calculations. However, the slopes are significantly different in the parallel and non-parallel stability theories. The phase distributions obtained with the NSE agree very well with the experiment in the whole region of measurements for all frequencies, while those obtained with the LPSE differ from both of them (see also Section 7.4). The

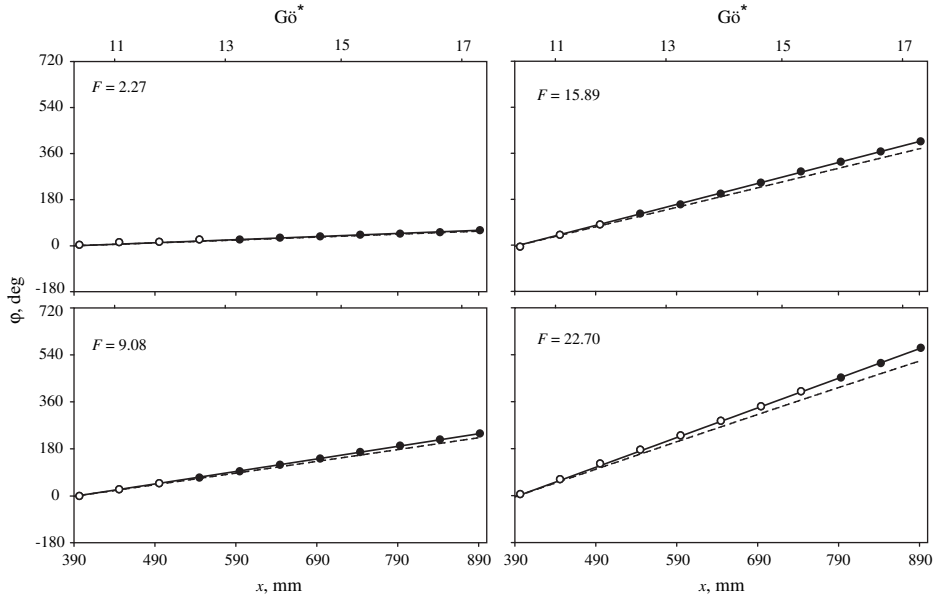

Fig. 16. Streamwise evolution of Görtler vortex phases for $\Lambda = 149$ and various frequencies obtained experimentally (circles) and numerically by NSE (–) and LPSE (– – –): far-field (●); near-field (○).

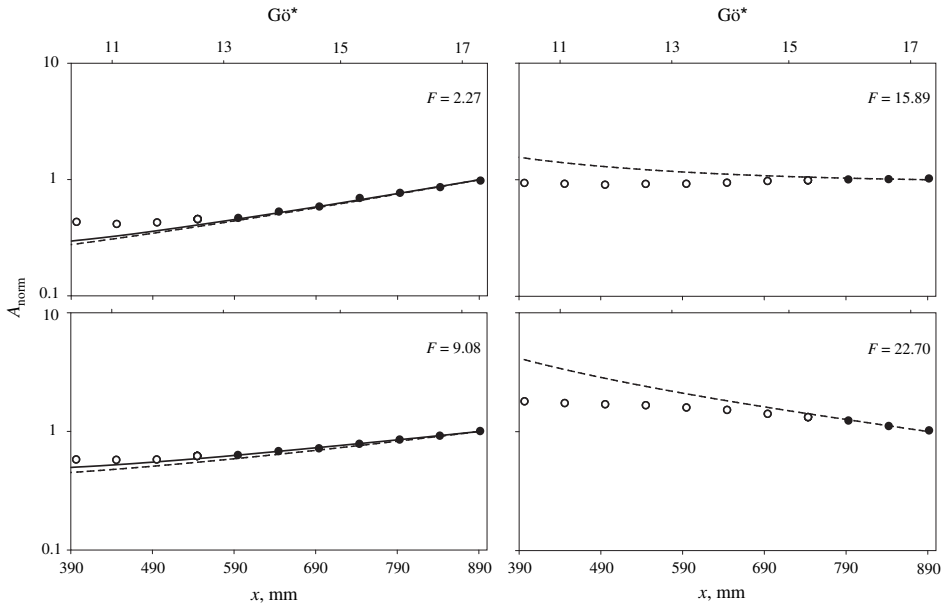

Fig. 17. Streamwise evolution of Görtler vortex amplitudes for $\Lambda = 775$ and various frequencies obtained experimentally (circles) and numerically by NSE (–) and LPSE (– – –): far-field (●); near-field (○).

absolute deviation of the phases is almost invisible for low frequencies but increases with frequency.

At spanwise wavelength $\Lambda = 274$ the streamwise amplitude and phase distributions were obtained, in addition, for an extremely low value of frequency parameter $F = 0.57$ ($f = 0.5$ Hz). The general picture of the downstream evolution of disturbances is found to be the same at this Λ as that observed at $\Lambda = 149$ (not shown). Again, there is a very good agreement between the experimental and numerical results observed for the two theoretical approaches in a wide range of the streamwise coordinates and frequencies excluding cases of weakly growing first-mode Görtler vortices (at $F = 19.29$ and 22.7). The NSE-approach predicts normally somewhat better the experimental results for all frequencies (basically for the phase distributions). Again, the growth of disturbance amplitude decreases with frequency, while the phase growth increases. At the same time, there is no any differences, practically, between amplification of vortices with $F = 2.27$, 0.57, and 0 (not shown). For vortices with this spanwise wavelength ($\Lambda = 274$) the upstream region, where the deviation between the experimental and theoretical results occurs (due to the source near-field), becomes quite pronounced on the plots of phase distributions, while at $\Lambda = 149$ (Fig. 16) it is practically invisible.

Everything aforesaid about the growing Görtler vortices with $\Lambda = 149$ and 274 is equally applicable to the distributions obtained for $\Lambda = 775$ (Figs. 17 and 18) with low frequencies up to $F = 9.08$. At higher frequencies the vortical amplitudes grow only slowly and

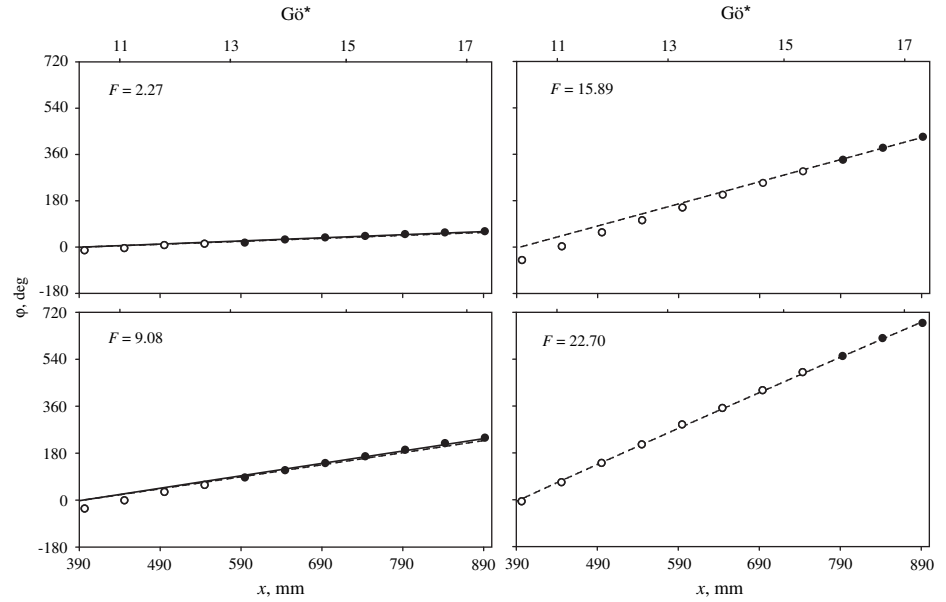

Fig. 18. Streamwise evolution of Görtler vortex phases for $\Lambda = 775$ and various frequencies obtained experimentally (circles) and numerically by NSE (–) and LPSE (– – –): far-field (●); near-field (○).

start to decay continuously at $F \geq 19.29$. The difficulties with extraction of the first discrete Görtler-instability mode during the NSE-calculations become the most topical for these vortices. However, in spite of the admixture of transients, identified in these calculations at high frequencies, the experimental streamwise distributions do not change their general behavior similar to that of Görtler vortices at other spanwise wavelengths. Moreover, the disturbance wall-normal profiles have qualitatively the same characteristic shapes being in accordance with the first Görtler-mode eigenfunctions calculated by means of the LPSE for attenuating vortices (Section 6.1). Due to this, it is natural to assume that even in these regimes of excitation we still observe in the experiment the predominance of the same first unsteady Görtler-instability mode. Therefore, only the LPSE-calculations can be used for correct comparison with the experimental data in the considered range of parameters. Indeed, at $F = 12.48$ the LPSE-amplification curves coincide, in fact, with the experimental ones (not shown). At $F = 15.89$ the experimental points demonstrate practically neutral behavior; the LPSE-amplitudes attenuate initially, but also display approximately neutral behavior in the end of the region of measurements (Fig. 17). At higher frequencies both the experimental and the LPSE-amplitudes attenuate everywhere, displaying qualitatively similar behavior, although the quantitative agreement is observed only in the very end of the region of measurements (in the source far-field).

Thus, an excellent quantitative agreement between the experimental and theoretical streamwise distributions of amplitudes and phases of Görtler vortices discussed above is obtained (for growing disturbances) in a wide range of spanwise wavelengthes and frequencies.

The characteristics of downstream development of Görtler vortices depend essentially on parameters of the problem. For instance, for each Λ the boundary layer is less stable to steady and quasi-steady vortices, amplitudes of which grow faster than those of essentially unsteady ones. This experimental and numerical result is consistent with that obtained theoretically in Ref. [20] for asymptotically large spanwise wavenumbers (i.e. for very small spanwise wavelengths) of steady vortices. In the range of disturbance parameters considered in the present study the influence of frequency is the strongest at the largest (of studied) spanwise wavelength $\Lambda = 775$ (i.e. for the smallest spanwise wavenumber). Indeed, at $\Lambda = 149$ to 274 the disturbance growth disappears at the highest studied frequency $F = 22.70$ only, while at $\Lambda = 775$ the growth stops as early as at $F = 15.89$.

In the low-frequency range $F = 0$–2.27 the disturbance amplification is practically independent of frequency. This is equally observed experimentally (for $F = 0.57$–2.27) and numerically; the same is true also for the disturbance eigenfunctions and the measured wall-normal amplitude profiles (Section 6.1). This is the range of quasi-stationary Görtler vortices, which corresponds physically to stationary vortices considered in numerous previous studies. Consequently, all results obtained in the present work at $F = 0.57$ and 2.27 correspond to the classic problem of steady Görtler instability (see also Sections 7.5 and 8).

7.4. Phase velocities of Görtler vortices

As has been shown above, the phases of the disturbances under study increase downstream in a nearly linear way both in the experiment and in the calculations. This fact gives us the possibility to obtain rather accurately the averaged phase velocities c_{ph} of the unsteady first Görtler modes by means of approximation of the streamwise phase distributions with straight lines performed in the disturbance source far-field. The obtained phase velocities correspond approximately to some mean values for the middle of the interval of averaging for $Gö^* \approx 15$. The same averaging procedure was applied to both the experimental and numerical distributions. The resulting frequency dependencies of the mean phase velocities of unsteady Görtler vortices are presented in Fig. 19a–c for $\Lambda = 149$, 274, and 775, respectively.

At $\Lambda = 149$ and 274 (Fig. 19a and b) it is clearly seen that the LPSE-approach overestimates somewhat the phase velocities compared to the experimental values, while the NSE-approach displays much better agreement with the experiment. It looks like the NSE-phase velocities are somewhat higher than the experimental ones, but the observed deviation seems to be connected mainly with a restricted accuracy of differentiation of the experimental data during estimation of the phase velocities. The phase velocities have values between 0.60 and 0.65, and at $\Lambda = 149$ and 274 depend slightly on frequency, increasing very slowly at $F > 5.67$ both in the experiment and in the calculations.

At the spanwise wavelength $\Lambda = 775$ (Fig. 19c) and $F \leq 9.08$ the situation with the frequency dependence of the phase velocities is approximately the same as that observed at $\Lambda = 149$ and 274. At higher frequencies only experiment and LPSE are able to provide adequate estimations of c_{ph}. According to the LPSE-calculations, the phase velocities of the nearly neutral and attenuating disturbances decrease with frequency and at $F = 19.29$ and 20.70 approach the experimental values. The experimental phase velocities experience, in fact, no frequency dependence.

Note that the observed phase velocities (about 0.60–0.65) are quite close to propagation velocities of the algebraically growing flat-plate transient disturbances found in Ref. [55] at $F = 26.9$ in a range of $\beta \approx 0.5$ to 1.0, i.e. for the parameters, which are quite close to those in the present study. However, in all studied cases the streamwise behavior of the disturbance amplitude is exponential, rather than algebraic, and the amplitude maximum of Görtler vortices in the wall-normal profiles correspond approximately to the location of the critical layer (i.e. to the wall distance where the disturbance phase velocity is equal to the local mean-flow velocity), rather than to the location of maximum of the transient disturbance amplitudes (see Section 6.1).

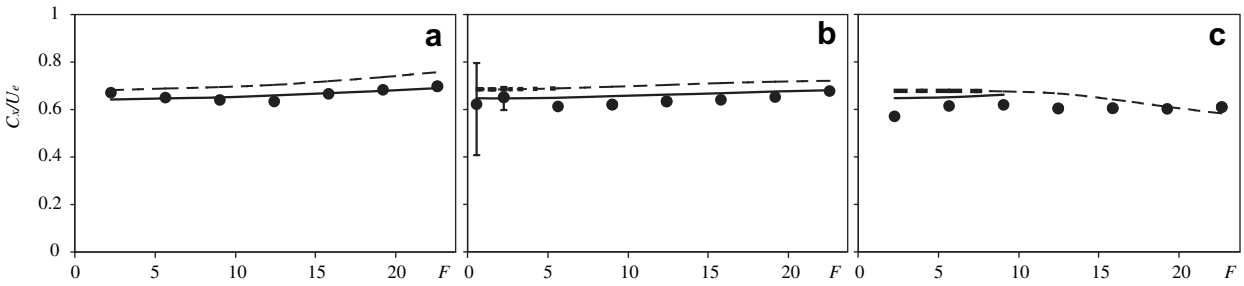

Fig. 19. Experimental (●), NSE (–) and LPSE (- - -) phase velocities of Görtler vortices averaged in the disturbance-source far-field (around $Gö^* \approx 15$) vs. frequency parameter at $\Lambda = 149$ (a); 274 (b); and 775 (c).

7.5. Amplification rates of Görtler vortices

The unsteady Görtler vortex increments averaged in the disturbance source far-field (around $G\ddot{o}^* \approx 15$) are shown in Fig. 20 versus frequency parameter for all three spanwise wavelengths studied. These increments are obtained similar to the phase velocities discussed above, but the approximation was performed for logarithms of disturbance amplitudes.

At $\Lambda = 149$ and 274 (Fig. 20a and b) the increments decay with frequency and the flow becomes neutrally stable at $F \approx 22.70$. Despite the quite strong frequency dependence, the variations of the increments at frequencies $F \gtrsim 2.27$ corresponded to the quasi-steady vortices are extremely weak. In general, the two theoretical approaches agree very well with the measurements, although the distribution given by the LPSE at $\Lambda = 149$ shows somewhat steeper slope, than those measured and calculated with the NSE. A significant distinction between calculated and measured increments is observed only at the highest studied frequencies $F = 19.29$ for $\Lambda = 149$, and $F = 19.29$ and 22.70 for $\Lambda = 274$, where the Görtler vortices display nearly neutral behavior and their selection from transient (near-field) disturbances of the same frequency becomes less efficient.

At $\Lambda = 775$ (Fig. 20c) the frequency dependence of the disturbance increments is qualitatively similar to those obtained for $\Lambda = 149$ and 274. However, the increments have significantly lower values. A good agreement of the experimental and the theoretical data is observed for the growing disturbances until $F = 9.08$ (NSE) and 12.48 (LPSE). Subsequent reduction of increments with frequency, observed in the experiment for nearly neutral and decaying disturbances, also corresponds qualitatively to the LPSE-results. The excess of the measured increments over the LPSE-ones in this region is explained by the base-flow non-parallelism or/and by admixture of transient disturbances in the experiment.

8. Stability diagrams

The results discussed above have shown that the LPSE describe quite adequately the growth rates of the disturbances under study. Inclusion of terms responsible for non-parallel effects improves the correspondence of the numerical and experimental data. Therefore, in this section we present data obtained with LNSE, which includes most of the non-local terms in the framework of modal analysis in the sense of Ref. [19].

8.1. Stability diagrams for steady and quasi-steady vortices

The Görtler instability diagrams obtained for steady and low-frequency disturbances are presented in Fig. 21 in the $(G\ddot{o}^*,\Lambda)$-plane for frequency parameters $F = 0$, 0.57, and 2.27. The calculated neutral stability curves and the equally spaced contour-lines of amplification rates (for growing disturbances only) are shown there for the Blasius boundary layer. As was indicated in Section 4, the slight deviation of the base flow studied in the present experiments from the Blasius one does not influence practically the amplification rates of Görtler-instability modes. Solid and dashed curves display the results obtained for the most amplified modes. Gray-tone areas display regions of instability calculated for the second discrete Görtler mode. Open circles indicate regions, in which the amplified first-mode Görtler vortices are found experimentally at $F = 0.57$ and 2.27.

It is seen that at $F = 0.57$ the stability diagram coincides with that obtained for steady Görtler vortices at $F = 0$ in the range of parameters shown. This is also true for $F = 2.27$ excluding a fringe region, in particular at $\Lambda \gtrsim 2000$ and $G\ddot{o}^* \gtrsim 40$. No deviation is observed in the central part of the stability diagrams corresponding to the most amplified (for every given $G\ddot{o}^*$) Görtler vortices including the regions of measurements, where the measured vortex amplitudes are amplified downstream in agreement with the theoretical results (see Sections. 7.3 and 7.5).

Thus, as has been already concluded in Section 6.2, the quasi-steady approach used in the present experiments for investigation of steady Görtler vortices works accurately in a wide range of practically interesting parameters. This makes it possible both to diminish the amplitudes of disturbances under study by two-three orders of magnitude and to increase, simultaneously, the accuracy of measurements by the two-three orders of magnitude.

Regions of amplification of the second discrete Görtler mode (shown in Fig. 21 with gray-tone areas) display that the flow becomes unstable to this mode only at $G\ddot{o}^* \gtrsim 14$. This instability is virtually absent for the largest disturbance spanwise wavelength studied experimentally and appears only by the end of the streamwise range investigated at two shorter wavelengths. Taking into account that the amplification of the second-mode is much smaller than that of the first one, this observation indicates that the second Görtler mode cannot become dominant in the flow at conditions of the present experiment and numerical calculations (based on the NSE-approach), if this mode is weak from the very beginning. The calculations have shown also (see Section 5) that the studied flow is always stable to the third and higher discrete Görtler modes within the range of the measurements.

8.2. Stability diagrams for essentially unsteady Görtler vortices

The stability diagrams obtained for essentially unsteady disturbances are presented in Fig. 22. It turned out that at high frequencies ($F \gtrsim 5$) another type of instability can be present in the boundary layer under study. This is the Tollmien–Schlichting (TS) mode, which is clearly observed at the present surface curvature at $\Lambda > 2000$ around Görtler number of several tens (Fig. 22) corresponding in the present study to Re^* of about 2000–3000. The connection between unsteady Görtler- and very oblique TS-modes has been shown in Ref. [56] based on an asymptotic approach at $G\ddot{o} \to 0$.

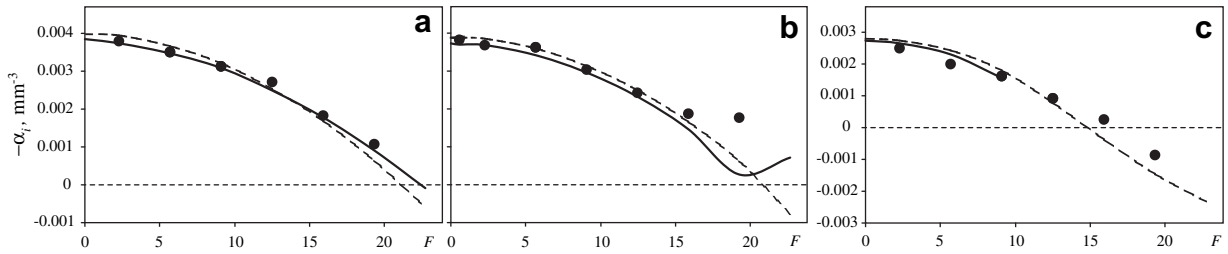

Fig. 20. Experimental (●), NSE (–) and LPSE (- - -) increments of Görtler vortices averaged in the disturbance-source far-field (around $G\ddot{o}^* \approx 15$) vs. frequency parameter at $\Lambda = 149$ (a); 274 (b); and 775 (c).

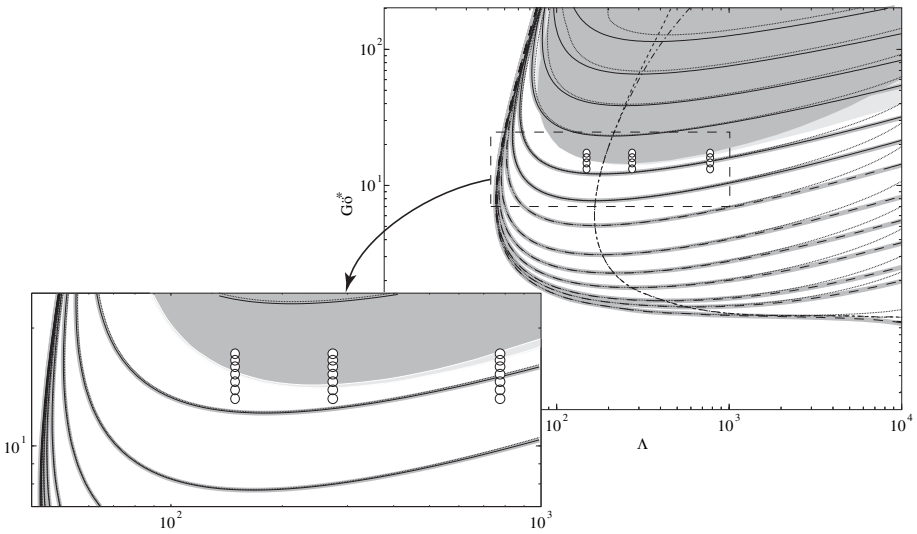

Fig. 21. Frequency dependence of Görtler instability diagram for steady and quasi-steady vortices with $F = 0$ (thick gray solid lines and light-gray area), $F = 0.57$ (solid lines and the same light-gray area), and $F = 2.27$ (dotted lines and dark gray area). Gray-tone areas show instability regions for the second discrete Görtler mode. Open circles indicate regions in which the amplified first-mode Görtler vortices are found in the experiment at $F = 0.57$ and 2.27. Dashed curve displays the line of maximum growth for $F = 0$ and 0.57; dash-dotted curve is the same line for $F = 2.27$.

However, the TS-instability is of viscous type, i.e. depends on viscosity (the Reynolds number). This is in contrast to the inviscid Görtler instability, for which surface curvature, rather than Reynolds number, is important. Less oblique TS-waves in a flat-plate boundary layer are usually considered to have a streamwise scale which is substantially different from that of Görtler vortices, being of order of the boundary-layer thickness δ. This implies fast oscillatory streamwise variations of the disturbances, i.e. $\alpha_r \sim 1/\delta$. As far as $\omega = \alpha_r c_{\mathrm{ph}}$, the assumption that c_{ph} is of order of the free-stream velocity U_0 leads to the TS-wave angular frequency $\omega \sim U_0/\delta$.

As the disturbances under study are oscillatory, the question arises on whether one can attribute them purely to the Görtler-, rather than to TS-instability? To this end a rigorous analysis of orders of magnitude of the amplitude functions, wavenumbers, and angular frequency was carried out based on their scalings in a way similar to that performed in Ref. [57] for transient disturbances and TS-waves. The analysis shows that to be able to formulate a common set of the locally non-parallel stability equations for the Görtler and TS instabilities of any oblique orientation, one has to preserve the streamwise pressure gradient term and the terms with squared streamwise wavenumber in linearized stability equations given in Part 1. This yields

$$i\alpha\hat{u} + \hat{v}_y + \beta\hat{w} = 0, \tag{14}$$

$$U_x\hat{u} + i\alpha U\hat{u} + V\hat{u}_y + U_y\hat{v} + \frac{i\alpha}{\mathrm{Re}^2}\hat{p} = \hat{u}_{yy} - \frac{\alpha^2}{\mathrm{Re}^2}\hat{u} - \beta^2\hat{u} + i\omega\hat{u}, \tag{15}$$

$$i\alpha U\hat{v} + V_x\hat{u} + V\hat{v}_y + V_y\hat{v} + 2G\ddot{o}^2U\hat{u} + \hat{p}_y = \hat{v}_{yy} - \frac{\alpha^2}{Re^2}\hat{v} - \beta^2\hat{v} + i\omega\hat{v}, \tag{16}$$

$$i\alpha U\hat{w} + V\hat{w}_y - \beta\hat{p} = \hat{w}_{yy} - \frac{\alpha^2}{Re^2}\hat{w} - \beta^2\hat{w} + i\omega\hat{w}, \tag{17}$$

where it is assumed that $Re = U_0\delta/\nu$ and $\delta = x/\sqrt{Re_x}$. Note that this set of equations depends both on Re and $G\ddot{o}$. This means that it is impossible to draw a universal neutral stability curve on the ($G\ddot{o}$,Λ)-plane at fixed frequency parameter F; instead one have to plot a three-dimensional surface in coordinates ($G\ddot{o}$,Λ,Re) or ($G\ddot{o}$,Λ,R) , where R is the dimensional radius of curvature.

Shown in Fig. 22 are some cuts of the surfaces of constant amplification rates corresponding to the experimental radius of curvature $R = 8.37$ m. Such representation allows to preserve both Görtler and Reynolds number axes on one graph. The diagrams were obtained on solving eqs. (14)–(17) by transforming the nonlinear eigenvalue problem to a standard form with the companion matrix method and application of QR-algorithm to find α. Details of the numerical approximation are described above. As usual in this paper, the data are renormalized using displacement thickness $\delta^* = 1.72\delta$ for easier comparison with the experiment.

Solid curves in Fig. 22 display the results obtained for the most amplified mode. The regions of the TS-wave instability calculated with the Orr–Sommerfeld equations are given with dark-tone gray areas. The regions of the second-mode instability are shown in light-gray. The experimentally observed growing and attenuating disturbances are presented with open and filled symbols respectively, while the experimental neutral points are indicated with asterisks. It is interesting also that the necessary condition of $\beta > \mathcal{O}(1)$ for the validity of local non-parallel approach can be probably omitted at least for $F \geq 15.89$, as the Görtler instability is just absent there. Hence, it is reasonable to assume that the right-hand side part of the plots is valid everywhere, except for the region of low Görtler numbers.

Note that the TS-instability domain ($G\ddot{o}^* \gtrsim 25$ and $\Lambda \gtrsim 2500$ at $F = 22.70$ or even further for lower frequencies) is located far away from the region of measurements and can not influence the experimental results in any case. Moreover, the instability diagrams calculated by means of LNSE (not shown) coincide with the presented curves everywhere except for a vicinity of the TS-wave instability region, where they, indeed, showed crude results. Note also that for all frequencies the disturbances with $\Lambda = 149$ and 274, studied in detail in the present work, are located close to the curve of maximum amplification shown in Fig. 22 with dashed line. These results provide an additional strong support that our experiments are related mainly to the first-mode Görtler instability. However, generally speaking, at larger Reynolds numbers and large spanwise

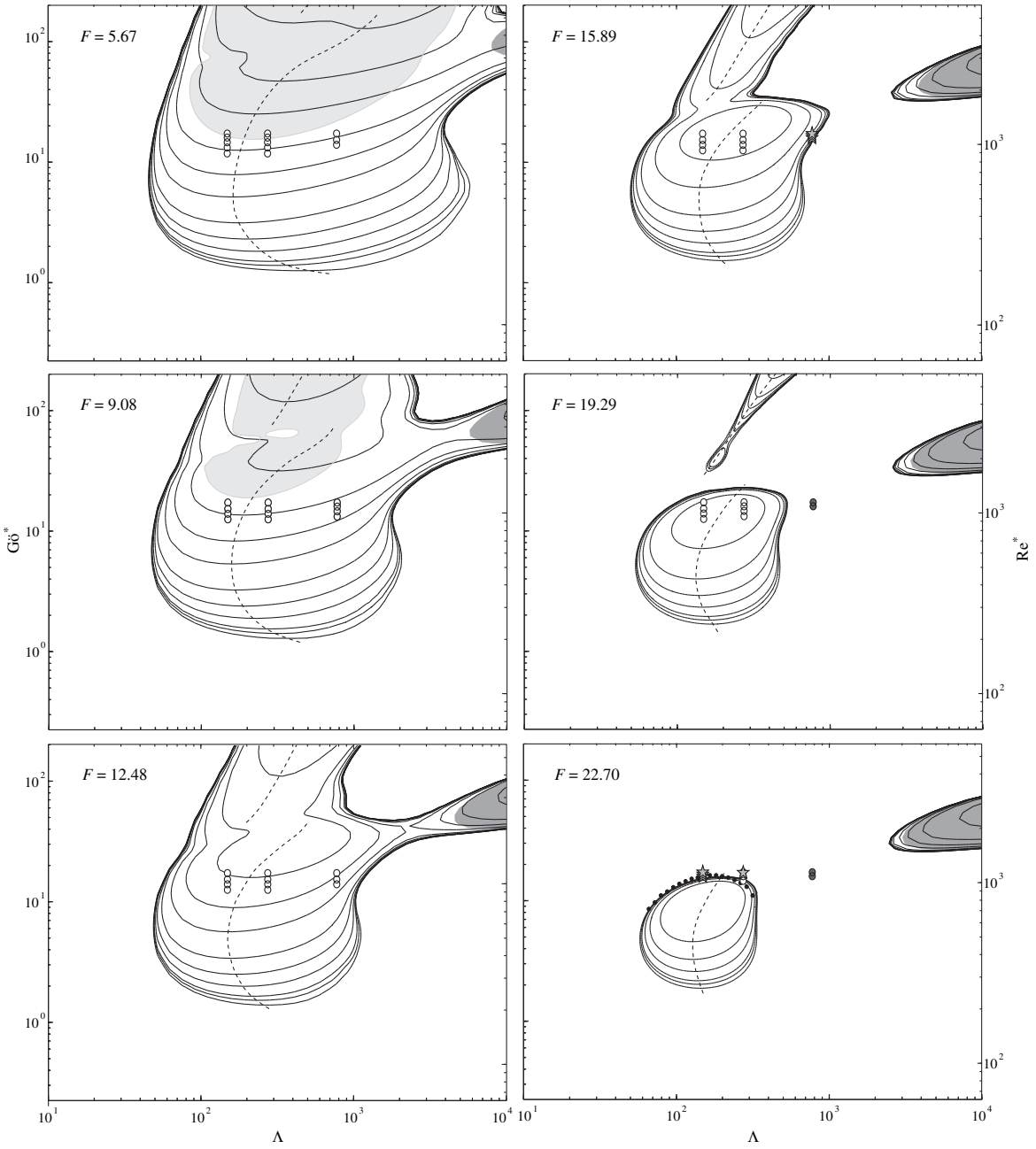

Fig. 22. Frequency dependence of Görtler instability diagram for moderate and high frequencies. Light-gray areas show instability regions for the second Görtler mode. Dark gray areas display regions of TS-instability obtained by solving the OS-equation. Dotted curve indicates the line of maximum growth. Dots show results of NSE-calculations. Open and filled symbols display amplified and attenuating disturbances in experiment; asterisks show experimentally detected neutral stability points. Contours – $\alpha_i = 0$; 0.01; 0.02; 0.05; 0.1; 0.2; 0.5; 1; 2; 5; 10; 20; and 40 are shown.

wavelength the boundary between these instabilities is fuzzy, i.e. the regions of both instabilities can overlap in a specific range of F, Λ, $Gö$ and Re in a qualitative agreement with the results of analysis made in Ref. [33], where growth of TS-waves was studied on a curved surface. As seen, the curvature enlarges a little bit the region of the TS-wave instability, that also was found in Ref. [33].

As frequency grows, the stability diagram undergoes significant changes. At $F = 5.67$ the flow becomes more stable to disturbances with $\Lambda \gtrsim 1000$ and $Gö^* \gtrsim 40$ (or $Re^* \gtrsim 2000$). At higher frequencies the instability region continues to shrink and by $F = 19.29$ it splits into three domains. One of them disappears at $F = 22.70$, while two others remain. As shown above, the domain located at relatively high Görtler numbers and large spanwise wavelengths corresponds to the TS-instability. The domain, located in the center of the plots (at moderate values of both Görtler number and spanwise wavelength), corresponds to the first discrete mode of Görtler instability, which represents the main object of the present study.

The experimental results presented in Fig. 22 are in excellent agreement with the calculated stability diagrams and corroborate them for all studied frequencies. At frequencies $F \leq 12.48$ the experimentally studied perturbations are amplified at all covered spanwise wavelengths and Görtler numbers. The first neutral stability point is found experimentally for vortices with $\Lambda = 775$ at $F = 15.89$ (the asterisk on the diagram corresponds to the neutral

stability point determined experimentally). As seen the location of this experimental point agrees very well with the calculated one. At $F = 19.29$ the disturbances with this Λ attenuate at all values of Görtler number in both the experiment and the theory. Similarly, at $F = 22.70$ the disturbances with the shorter measured spanwise wavelengths ($\Lambda = 149$ and 274) exhibit appearance of neutral points at $G\ddot{o}^* \approx 16$ in complete agreement with the calculations. A small deviation between location of the experimental and theoretical neutral points can be attributed to some effects of the base-flow non-parallelism, since in the LPSE-calculations they are taken into account only partly (in contrast to NSE). In order to estimate possible influence of the flow non-parallelism on the location of the upper part of the neutral curve, the NSE-calculations were performed. Their results are presented for $F = 22.70$ by circles. As seen the NSE-approach gives only a very little displacement of the neutral curve, providing a somewhat better agreement with the experiment for $\Lambda = 149$.

Starting with $F = 19.29$ the domain corresponding to the amplifying first Görtler mode located in the center of the plots becomes isolated occupying a restricted area on the stability diagram. For instance, at $F = 22.70$ the flow is unstable only at $1.9 \lesssim G\ddot{o}^* \lesssim 16$. This means, in particular, that an *increase* of Görtler number is able to *stabilize* the flow with respect to the first-mode Görtler vortices with all spanwise wavenumbers and given fixed frequency! This result is a paradoxical one. Indeed, the Görtler number is proportional to square root of the surface curvature, i.e. $G\ddot{o}^* \sim (1/R)^{1/2}$. Therefore, its growth can be interpreted as a relative increase of the wall curvature and, hence, an increase of centrifugal forces, which represent the main cause of the Görtler instability. However, this growth is shown to be able to lead to the flow stabilization. The only "visible" cause of this phenomenon might be associated with the air viscosity, which provides a stabilization for the unsteady Görtler vortices at least in the region of frequencies and Reynolds numbers characteristic for the TS-instability, the stabilization being increased with F and Re.

Note in the end that amplification of the second discrete Görtler mode, shown in Fig. 22 with light-gray-tone areas, occurs in the given range of parameters at $F \leq 9.08$ only. Moreover, even at these frequencies the second-mode can be amplified at quite high Görtler numbers only and can not play any significant role in the measurements. The calculations indicate also that the flow is always stable to all higher discrete Görtler modes within the studied range of parameters.

9. Conclusions

In the present study all characteristics of linear-stability of a boundary layer on concave wall to the leading discrete-spectrum Görtler mode were obtained experimentally for both the steady (within the quasi-stationary approach) and unsteady vortices. A detailed investigation is performed in 22 excitation regimes for three spanwise wavelengths $\Lambda = 149$, 274, and 775 in the ranges of values of local Görtler number $G\ddot{o}^* = 10.3$–17.3 and frequency parameter $F = 0.57$–22.70. Similar results were obtained numerically for the experimental conditions within the framework of three theoretical approaches based on the locally-parallel and the non-parallel stability theories (eigenvalue problems) and on numerical solution of initial-valuer problem based on parabolic stability equations.

In contrast to previous measurements of steady Görtler vortices, all present experimental results were obtained for very low-amplitude disturbances with initial amplitudes for the largest streamwise-velocity component of several hundredth or tenth of a percent of the free-stream speed. The characteristics of the disturbance development are shown to be independent of the amplitude up to 3% of U_e (at least), hence proving the linearity of the investigated instability mechanisms.

The following most important results are obtained in the present study.

Methodological results obtained

1. A new experimental approach is developed and applied to investigation of stationary and non-stationary linear Görtler instability. This approach includes: (*i*) the quasi-steady method of investigation of stationary Görtler-vortex instability, (*ii*) a new, very efficient, method of excitation of controlled quasi-steady and unsteady Görtler vortices, (*iii*) utilizing of optimized experimental model and regimes of measurements providing absence of any significant uncontrolled Görtler modes, and (*iv*) accurate treatment of the disturbance-source near-field. The applicability and very high efficiency of this approach is substantiated both experimentally and theoretically.
2. In particular, it is shown that the tuning-out of the exact zero frequency, applied within the framework of the quasi-steady method, gives the possibility to diminish the disturbance amplitude (compared to previous experiments) by two-three orders of magnitude and, simultaneously, to increase the measurement accuracy by approximately the same orders. It is found also that the quasi-steady method works very well and provides the possibility of accurate investigation of the linear boundary-layer instability to physically stationary Görtler vortices.
3. For the first time quasi-steady and essentially unsteady controlled Görtler vortices were excited by a disturbance source used previously for excitation of TS- and cross-flow waves. The source is shown to be able to generate boundary-layer perturbations corresponding mainly to the first (most dangerous) Görtler-instability mode with a quite short near-field region (where other modes are admixed). Due to these properties, the source can be used in future for excitation of various combinations of the indicated types of instability modes for investigation of their simultaneous development and interaction.
4. Three theoretical approaches to the linear unsteady (in general) Görtler instability are developed based on: (*i*) locally-parallel linear-stability equations (LPSE), (*ii*) locally non-parallel stability equations (LNSE), and (*iii*) essentially non-local non-parallel stability equations (NSE). Their numerical implementations made it possible to perform for the first time a systematic theoretical and numerical investigation of characteristics of boundary-layer linear-stability to unsteady Görtler vortices. These theoretical approaches help also significantly in substantiation of the used experimental approach and in selection of optimal experimental regimes and parameters.

Main scientific results obtained

1. For the first time an accurate correspondence between the experimental and theoretical linear-stability characteristics was obtained for steady Görtler vortices outside the disturbance-source near-field (having length up to two hundred boundary-layer displacement thicknesses downstream of the source).
2. Similarly, a very good agreement is obtained for unsteady Görtler vortices (corresponded also to the most dangerous first discrete Görtler mode).
3. The experimental wall-normal profiles of the disturbance amplitudes and phases measured in the range $13 \lesssim G\ddot{o} \leq 17.3$ are found to agree very well, in the disturbance-source far-field, with eigenfunctions of the first mode of Görtler instability both for steady and unsteady vortices. For growing steady and unsteady first-mode Görtler vortices the two applied

theoretical approaches are shown to predict very well the experimental shapes of the disturbances. However, the approach based on the non-parallel stability equations (NSE) predicts them somewhat better then the approach based on the locally-parallel stability equations (LPSE).

4. At low frequencies, the spectrum of the eigenvalue problem solved for the Blasius boundary layer developing over concave surface is found to be similar to that solved for the corresponding steady problem. It consists of several (in general) discrete Görtler modes (some of which can be amplified) and continuous-spectrum modes (always attenuating).
5. Eigenfunction *amplitude* profiles of the unsteady Görtler vortices corresponding to the most dangerous first discrete mode are found to be very similar to those of the steady ones, quite conservative (in the range of studied parameters), and to have one maximum near the critical layer, which location displaces weakly away from the wall with frequency and spanwise wavelength and moves towards the wall with local Görtler number.
6. Eigenfunction *phase* profiles of unsteady first-mode Görtler vortices are found to display a quasi-linear phase decay with the wall-normal coordinate, which rate increases with the disturbance frequency almost proportionally. There is also a weak increase of this decay rate with spanwise wavelength and local Görtler number.
7. The comparative analysis of shapes of the steady and unsteady perturbations has shown that the quasi-steady first Görtler mode corresponds to the well-known steady one and represents one layer (in wall-normal direction) of counter-rotating vortices (distributed in spanwise direction) with their axes parallel to the wall; the vortices change the direction of their rotation periodically in time. Meanwhile, the essentially unsteady first-mode Görtler vortices are inclined to the wall at angles increasing with frequency and appear one above the other resulting in formation of several counter-rotating vortex layers located at different distances from the wall.
8. It is found that non-local, non-parallel linear-stability theory predicts better the characteristics of the boundary-layer instability to both stationary and non-stationary unstable Görtler vortices. However, the disturbance growth rates are predicted fairly well by the locally-parallel linear-stability theory as well.
9. The amplification rates of unsteady Görtler vortices decrease, in general, with frequency, but at low frequencies this reduction is very weak and the disturbance behavior corresponds to quasi-steady one.
10. Phase velocities of unsteady Görtler vortices turned out to be close to 0.60–0.65 and depend only marginally on the base-flow and disturbance parameters.
11. At quasi-steady frequencies (similar to the case of zero frequency) the instability region observed on the stability diagram represents a single domain (at least at $G\ddot{o}^* \leq 200$ and $\Lambda \leq 10^4$). At higher frequencies this region is split into two and then three domains. One of them, located at the lowest Görtler numbers (between several units to about 20), corresponds to the first unsteady Görtler mode and shrinks gradually with frequency. The domain located at large spanwise wavelengthes corresponds to the TS-instability (with strongly oblique TS-waves) and remains at high frequencies, including those at which the Görtler instability is absent.
12. A paradoxical result is obtained that growth of Görtler number is able to stabilize the flow with respect to unsteady Görtler vortices. The Görtler instability can be present for a given frequency at $G\ddot{o}^*$ of several units but absent (for all spanwise scales) at $G\ddot{o}^*$ of several tens and even hundreds.

Acknowledgements

This work is supported by the Russian Foundation for Basic Research (grant No 06-01-00519).

References

[1] P.G. Drazin, W.H. Reid, Hydrodynamic Stability. Cambridge University Press, Cambridge, 1981.
[2] P. Hall, Görtler vortices in growing boundary layers: the leading edge receptivity problem, linear growth and the nonlinear breakdown stage. Mathematika 37 (1990) 151.
[3] J.M. Floryan, On the Görtler instability of boundary layers. J. Aerosp. Sci. 28 (1991) 235.
[4] W.S. Saric, Görtler vortices. Annu. Rev. Fluid Mech. 26 (1994) 379.
[5] G.I. Taylor, Stability of a viscous liquid contained between two rotating cylinders. Proc. R. Soc. Lond. A 102 (1923) 541.
[6] M. Clauser, F. Clauser, The effect of curvature on the transition from laminar to turbulent boundary layer NACA TN 613 (1937).
[7] H. Görtler, Inistabilität laminaren Grenzschichten an konkaven Wänden gegenüber gewissen dreidimensionalen Störungen. Z. Angew. Math. Mech. 21 (1941) 250.
[8] H.W. Liepmann, Investigations on laminar boundary layer stability and transition on curved boundaries NACA Wartime Rep. W-107 (1943).
[9] N. Gregory, W.S. Walker, The effect on transition of isolated surface excrescences in the boundary-layer ARC R&M 2779 (1956).
[10] I. Tani, Production of longitudinal vortices in the boundary-layer along a curved wall. J. Geophys. Res. 67 (1962) 3075.
[11] A. Ito, "Visualization of boundary layer transition along a concave wall," in Proc. 4th Int. Symp. Flow Visualization (Hemisphere, Washington, 1987), pp. 339–344.
[12] H. Bippes, H. Görtler, Dreidimensionale Störungen in der Grenzschicht an einer konkaven Wand. Acta Mech. 14 (1972) 251.
[13] Y. Aihara, Y. Tomita, A. Ito, Generation, development and distortion of longitudinal vortices in boundary layers along concave and flat plates IUTAM Symposium. in: V.V. Kozlov (Ed.), Laminar–Turbulent Transition. Springer–Verlag, Berlin, 1985, pp. 447–454.
[14] Y. Tomita, K. Funatsu, S. Tsuzuki, K. Miyazaki, Neutral stability of laminar boundary layers along the concave wall. Bull. J. Jpn. Soc. Mech. Eng. 28 (1985) 2288.
[15] M.V. Finnis, A. Brown, The linear growth of görtler vortices. Int. J. Heat Fluid Flow 18 (1997) 389.
[16] G. Hämmerlin, Zur Theorie der dreidimensionalen Instabilität laminarer Grenzschichten. Z. Angew. Math. Phys. 7 (1956) 156.
[17] G. Hämmerlin, Über das Eigenwertproblem der dredimensionalen Instabilität laminarer Grenzschichten an konkaven Wänden. J. Rat. Mech. Anal. 4 (1955) 279.
[18] A.M.O. Smith, On the growth of Taylor–Görtler vortices along highly concave walls. Quart. Appl. Math. 13 (1955) 223.
[19] J.M. Floryan, W.S. Saric, Stability of Görtler vortices in boundary layers. AIAA J. 20 (1982) 316.
[20] P. Hall, Taylor–Görtler vortices in fully developed or boundary-layer flows: linear theory. J. Fluid Mech. 124 (1982) 475.
[21] P. Hall, The linear development of Görtler vortices in growing boundary layers,". J. Fluid Mech. 130 (1983) 41.
[22] P. Hall, The nonlinear development of Görtler vortices in growing boundary layers,". J. Fluid Mech. 193 (1988) 243.
[23] P. Luchini, A. Bottaro, Görtler vortices: a backward in time approach to the receptivity problem. J. Fluid Mech. 363 (1998) 1.
[24] A. Bottaro, P. Luchini, Görtler vortices: are they amenable to local eigenvalue analysis? Eur. J. Mech. B/Fluids 18 (1999) 47.
[25] J.P. Denier, P. Hall, S.O. Seddougui, On the receptivity problem for Görtler vortices: vortex motions induced by roughness. Philos. Trans. R. Soc. Lond. A 335 (1991) 51.
[26] A.P. Bassom, P. Hall, Concerning the interaction of non-stationary crossflow vortices in a three-dimensional boundary layer. Quart. J. Mech. Appl. Math. 44 (1991) 147.
[27] P. Andersson, M. Berggren, D.S. Henningson, Optimal disturbances and bypass transition in boundary layers. Phys. Fluids 11 (1999) 134.
[28] P. Luchini, Reynolds-number-independent instability of the boundary layer over a flat surface: optimal perturbations. J. Fluid Mech. 404 (2000) 289.
[29] P.J. Schmid, D.S. Henningson, Stability and Transition in Shear Flows. Springer–Verlag, Berlin, 2000.
[30] A. Tumin, E. Reshotko, Spatial theory of optimal disturbances in boundary layers. Phys. Fluids 13 (2001) 2097.
[31] I.H. Herron, A.D. Clark, Instabilities in the Görtler model for wall bounded flows. Appl. Math. Lett. 13 (2000) 105.
[32] R.E. Spall, M.R. Malik, Goertler vortices in supersonic boundary layers AIAA Paper 88–3678 (1988).
[33] F.P. Bertolotti, Vortex generation and wave-vortex interaction over a concave plate with roughness and suction ICASE Rep. 93–101 (1993).
[34] M.P. Schultz, R.J. Volino, Effects of concave curvature on boundary layer transition under high free-stream turbulence conditions. ASME J. Fluids Eng. 125 (2003) 18.

[35] V.R. Gaponenko, A.V. Ivanov, Y.S. Kachanov, J.D. Crouch, Swept-wing boundary-layer receptivity to surface non-uniformities. J. Fluid Mech. 461 (2002) 93.
[36] V.I. Borodulin, Y.S. Kachanov, D.B. Koptsev, Study of resonant instability wave interaction in self-similar boundary layer with adverse pressure gradient, in: Proc. X Internat. Conf. on Methods of Aerophysical Research, vol. 1. RAS. Sib. Branch Inst. Theoret. Appl. Mech., Novosibirsk, 2000, pp. 47–52.
[37] V.I. Borodulin, Y.S. Kachanov, D.B. Koptsev, Experimental study of resonant interactions of instability waves in self-similar boundary layer with an adverse pressure gradient: I. Tuned resonances. J. Turbulence 3 (2002) 1.
[38] V.I. Borodulin, Y.S. Kachanov, D.B. Koptsev, Experimental study of resonant interactions of instability waves in self-similar boundary layer with an adverse pressure gradient: III. Broadband disturbances. J. Turbulence 3 (2002) 1.
[39] V.I. Borodulin, Y.S. Kachanov, D.B. Koptsev, A.P. Roschektayev, Experimental study of resonant interactions of instability waves in self-similar boundary layer with an adverse pressure gradient: II. Detuned resonances. J. Turbulence 3 (2002) 1.
[40] V.I. Borodulin, V.R. Gaponenko, Y.S. Kachanov, Method of introduction of normal instability modes into the 3D boundary layer, in: , Proc. Eighth Internat. Conf. On methods of Aerophysical research, vol. 2. RAS. Sib. Branch Inst. Theoret. Appl. Mech., Novosibirsk, 1996, pp. 39–45.
[41] V.S. Kosorygin, Laboratory complex for manufacturing of miniature hot-wire probes with a heated wire No 4166–4182. Dep. in VINITI, Moscow, 1982.
[42] C. Canuto, M.Y. Hussaini, A. Quarteroni, T.A. Zang, Spectral Methods in Fluid Dynamics, Springer Series in Computational Physics. Springer–Verlag, Berlin, 1988.
[43] J.A.C. Weideman, S.C. Reddy, A MATLAB differentiation matrix suite,". ACM Trans. Math. Software 26 (2000) 465.
[44] C.B. Moler, G.W. Stewart, An algorithm for generalized matrix eigenvalue problems. SIAM J. Numer. Anal. 10 (1973) 241.
[45] B.G.B. Klingmann, A.V. Boiko, K.J.A. Westin, V.V. Kozlov, P.H. Alfredsson, Experiments on the stability of Tollmien–Schlichting waves. Eur. J. Mech. B/Fluids 12 (1993) 493.
[46] T. Cebeci, J. Cousteix, Modelling and Computation of Boundary Layer Flows. Springer–Verlag, Berlin, 1999.
[47] J.C. Tannehill, D.A. Anderson, R.H. Pletcher, Computational Fluid Mechanics and Heat Transfer, second ed. Taylor & Francis, 1997.
[48] J.M. Floryan, W.S. Saric, Wavelength selection and growth of Görtler vortices. AIAA J. 22 (1984) 1529.
[49] H.P. Day, T. Herbert, W.S. Saric, Comparing local and marching analyses of Görtler instability. AIAA J. 28 (1990) 1010.
[50] A.V. Boiko, A.V. Ivanov, Y.S. Kachanov, D.A. Mischenko, Quasi-steady and unsteady Görtler instability on concave wall: stability characteristics 00, 00. Phys. Fluids (2008).
[51] J.M. Floryan, Gortler instability of wall jets. AIAA J. 27 (1989) 112.
[52] K.J.A. Westin, A.A. Bakchinov, V.V. Kozlov, P.H. Alfredsson, Experiments on localized disturbances in a flat plate boundary layer. Part 1: the receptivity and evolution of a localized free stream disturbance. Eur. J. Mech. B/Fluids 17 (1998) 823.
[53] A.V. Boiko, Receptivity of a flat plate boundary layer to free stream axial vortex. Eur. J. Mech. B/Fluids 21 (2002) 325.
[54] Y.S. Kachanov, A. Michalke, Three-dimensional instability of flat-plate boundary layers: theory and experiment. Eur. J. Mech. B/Fluids 13 (1994) 401.
[55] A.V. Boiko, G.R. Grek, D.S. Sboev, Spectral analysis of localized disturbances in boundary layer at subcritical Reynolds numbers. Phys. Fluids 15 (2003) 3613.
[56] M. Choudhari, P. Hall, C.L. Streett, On the spatial evolution of long wavelength Görtler vortices governed by a viscous-inviscid interaction. Part 1: the linear case. Quart. J. Mech. Appl. Math. 47 (1994) 207.
[57] O. Levin, D.S. Henningson, Exponential vs algebraic growth and transition prediction in boundary layer flow. Tech. Rep. (2003).